IEEE Access
Multidisciplinary | Rapid Review | Open Access Journal

Received June 7, 2016, accepted June 30, 2016. Date of publication xxxx 00, 0000, date of current version xxxx 00, 0000.

Digital Object Identifier 10.1109/ACCESS.2016.2591903

Joint Quantum-Assisted Channel Estimation and Data Detection

PANAGIOTIS BOTSINIS, (Member, IEEE), DIMITRIOS ALANIS, (Student Member, IEEE), ZUNAIRA BABAR, SOON XIN NG, (Senior Member, IEEE), AND LAJOS HANZO, (Fellow, IEEE)

School of Electronics and Computer Science, University of Southampton, Southampton SO17 1BJ, U.K.

Corresponding author: L. Hanzo (lh@ecs.soton.ac.uk)

This work was supported in part by the European Research Council through the Advanced Fellow Grant, in part by the Royal Society's Wolfson Research Merit Award, and in part by the Engineering and Physical Sciences Research Council under Grant EP/L018659/1.

ABSTRACT Joint channel estimation (CE) and multi-user detection (MUD) have become a crucial part of iterative receivers. In this paper, we propose a quantum-assisted repeated weighted boosting search (QRWBS) algorithm for CE and we employ it in the uplink of multiple-input multiple-output orthogonal frequency division multiplexing systems, in conjunction with the maximum *a posteriori* probability (MAP) MUD and a near-optimal quantum-assisted MUD (QMUD). The performance of the QRWBS-aided CE is evaluated in rank-deficient systems, where the number of receive antenn elements (AEs) at the base station (BS) is lower than the number of supported users. The effect of the channel impulse response prediction filters, of the power delay profile of the channels, and of the Doppler frequency on the attainable system performance is also quantified. The proposed QRWBS-aided CE is shown to outperform the RWBS-aided CE, despite requiring a lower complexity, in systems where iterations are invoked between the MUD, the CE, and the channel decoders at the receiver. In a system, where $U = 7$ users are supported with the aid of $P = 4$ receive AEs, the joint QRWBS-aided CE and QMUD achieves a 2-dB gain, when compared with the joint RWBS-aided CE and MAP MUD, despite imposing 43% lower complexity.

INDEX TERMS Channel estimation, computational complexity, Dürr-Høyer algorithm, Grover's quantum search algorithm, multiuser detection, orthogonal frequency division multiplexing, prediction filter, quantum computing, repeated weighted boosting search.

LIST OF ABBREVIATIONS

ACO	Ant Colony Optimization
AE	Antenna Element
AWGN	Additive White Gaussian Noise
BS	Base Station
CDMA	Code Division Multiple Access
CE	Channel Estimation
CF	Cost Function
CFE	Cost Function Evaluation
CIR	Channel Impulse Response
CRC	Cyclic Redundancy Check
DDCE	Decision-Directed Channel Estimation
DEA	Differential Evolution Algorithm
DEC	Decoder
DHA	Dürr-Høyer Algorithm
ES	Early Stopping
ETU	Extended Typical Urban
EVA	Extended Vehicular A
FD-CHTF	Frequency-Domain CHannel Transfer Function
FFT	Fast Fourier Transform
FKT	Forward Knowledge Transfer
GA	Genetic Algorithm
HIHO	Hard-Input Hard-Output
IDMA	Interleave Division Multiple Access
IFFT	Inverse Fast Fourier Transform
JCEMUD	Joint Channel Estimation and Multi-User Detection
LLR	Log Likelihood Ratio
LS	Least Squares
MAP	Maximum A posteriori Probability
MIMO	Multiple-Input Multiple-Output
MMSE	Minimum Mean Square Error
MSE	Mean Square Error
MUA	MUlti-input Approximation

MUD	Multi-User Detection
MUI	Multi-User Interference
OFDM	Orthogonal Frequency Division Multiplexing
OHRSA	Optimised Hierarchy Reduced Search Algorithm
PDP	Power Delay Profile
PSO	Particle Swarm Optimization
QMUD	Quantum-assisted Multi-User Detection
QRWBS	Quantum-assisted Repeated Weighted Boosting Search
QSA	Quantum Search Algorithm
RWBS	Repeated Weighted Boosting Search
SDMA	Spatial Division Multiple Access
SISO	Soft-Input Soft-Output
WBS	Weighted Boosting Search
ZF	Zero-Forcing.

I. INTRODUCTION

In the uplink of high-velocity multi-user, multi-carrier systems, the complexity imposed by accurately estimating the channels, as well as detecting the transmitted symbols may become excessive. Hence the performance of compplexity-limited systems may degrade, especially when associated with a low number of receive Antenna Elements (AE) at the Base Station (BS), which results in rank-deficient scenarios [1], [2]. Various techniques have been proposed for providing Channel Estimation (CE) with the aid of pilot training symbols [3], [4] as well as low-complexity Multi-User Detection (MUD) [2], [5]–[7]. In [4], Li also proposed an optimal pilot sequence for minimizing the Mean Square Error (MSE) of the CE process.

The performance of a Multiple-Input Multiple-Output (MIMO) Orthogonal Frequency Division Multiplexing (OFDM) system was found to be improved when joint channel estimation and multi-user detection was used [8]–[15]. During the process of Decision-Directed Channel Estimation (DDCE) [1], [11] the CE benefits by exploiting the confidently detected high-reliability symbols of the MUD for improving the channel estimates. Soft-decision aided joint channel estimation and data detection [11], [16], [17] provide improved symbol and channel estimates, when compared to their hard-decision aided equivalents, where iterations exchanging soft extrinsic information are invoked between the MUD, the CE and the decoders. Since the search space of the channel estimation problem is continuous, joint turbo CE and MUD may be assisted by evolutionary algorithms, resulting in CEs such as the Genetic Algorithm (GA)-aided CE [10], [18], [19], and the Repeated Weighted Boosting Search (RWBS)-aided CE [17], as well as the Particle Swarm Optimization (PSO) aided CE [19] and the Differential Evolution Algorithm (DEA) aided CE [19], [20]. In [19], Zhang *et al.* employed discrete-space and continuous-space evolutionary algorithms in the MUD and the CE, respectively, for performing joint channel estimation and multi-user detection. Jiang *et al.* in [18] combined a GA-aided CE with the Optimised Hierarchy Reduced Search Algorithm (OHRSA) assisted MUD for providing joint CE and MUD. The main contributions in the field of joint channel estimation and data detection are summarized in Table 1.

Quantum computing [21]–[23] may support the process of joint CE and MUD by exploiting its inherent parallelism for reducing the complexity and for improving the data detection's and channel estimation's performance. Grover's Quantum Search Algorithm (QSA) [24], [25] succeeds in finding a wanted value in an unsorted database having N entries with as few as $O(\sqrt{N})$ queries to the database, provided that the number of times this wanted entry appears in the database is known *a priori*. Boyer *et al.* [26] improved Grover's QSA by finding the wanted value in the database without any prior knowledge of the number of times this ''solution'' appears in it, at the same order of complexity of $O(\sqrt{N})$ queries to the database. Furthermore, the Dürr-Høyer Algorithm (DHA) [27], which finds the specific argument that minimizes a function by using $O(\sqrt{N})$ function evaluations. In [28], Malossini *et al.* proposed the quantum-assisted genetic optimization algorithm and compared it to the GA. In our previous work we have proposed quantum-assisted algorithms for providing near-optimal hard-input hard-output (HIHO) Quantum-asissted MUDs (QMUD) [7], [29], as well as soft-input soft-output (SISO) QMUDs [7], [30]–[32], which may be employed in iterative receivers and indeed were found to be superior both to the conventional Zero-Forcing (ZF) and Minimum Mean Square Error (MMSE) detectors, as well as to the Ant Colony Optimization (ACO) [30]. In [33], we presented a non-coherent quantum-assisted multiple symbol differential detector, which may be used in systems, where channel estimation is not employed. Quantum computing may also be used in other fields of wireless communications, such as in routing [34], [35], as well as in quantum-domain based communications [36]–[39]. Quantum error correction is essential for extending the coherence-time of quantum circuits.

Against this background, our novel contributions are:

1) *We propose the novel Quantum-assisted Repeated Weighted Boosting Search (QRWBS), by amalgamating the DHA as well as the classical RWBS and we employ it in the context of providing accurate quantum-assisted CE in iterative receivers. We show our QRWBS-aided CE achieves a better performance than the classic RWBS-aided CE, despite its lower complexity. We demonstrate that the proposed quantum-assisted algorithm may be integrated with iterative receivers and we investigate various scenarios of multiple iterations between the MUD, the CE and the decoders, while identifying which specific iterations are more beneficial for the system's BER performance.*
2) *We intrinsically amalgamate the QRWBS-aided CE with the SISO DHA-aided QMUD relying on the MUlti-input Approximation and Forward Knowledge Transfer (DHA-MUA-FKT) based QMUD of [30] and [32] for conceiving a quantum-assisted joint channel*

TABLE 1. Selected contributions in joint channel estimation & data detection.

Year	Author(s)	Contribution
1992	Ghosh and Weber [8]	Proposed a joint channel estimator and data detector, relying on the least squares and maximum likelihood criteria, respectively.
1994	Seshadri [9]	Presented a recursive algorithm for joint channel estimation and data detection, using a different version of the Viterbi algorithm, where multiple surviving paths are considered.
1998	Chen and Wu [10]	Developed a joint channel and data estimation based on the GA.
2004	So and Cheng [12]	Proposed a joint channel and data estimator based on the expectation-maximization algorithm for MIMO frequency-selective fading channels.
2007	Jiang *et al.* [18]	Presented a GA-aided joint channel and multi-user data estimator for rank-deficient MIMO-OFDM scenarios.
2010	Assra *et al.* [13]	Provided a closed-form expression for the expectation-maximization algorithm's weight coefficients, when employed for joint channel and data estimation in MIMO Code Division Multiple Access (CDMA) systems.
2011	Zhang *et al.* [17]	Implemented a soft-output joint channel estimator and multi-user detector, with the aid of the dual RWBS algorithm, allowing iterations both between the channel estimator and the multi-user detector, as well as between the joint estimation procedure and the channel decoders in Spatial Division Multiple Access (SDMA)-OFDM systems.
2012	Zhang *et al.* [20]	Developed an iterative DEA-aided joint channel estimator and multi-user detector, allowing the exchange of updated channel and multi-user symbol estimates between the channel estimator and the multi-user detector in SDMA-OFDM systems.
2013	Novak *et al.* [14]	Suggested a joint channel estimator and data detector using the factor-graph framework in Interleave Division Multiple Access (IDMA)-OFDM systems.
2014	Zhang *et al.* [11]	Proposed an iterative joint channel and data estimator in MIMO systems, which only exploits the high-quality soft symbol outputs of the data detector for further iterations of channel estimation, while also allowing iterations between the joint estimation procedure and the channel decoders.
	Zhang *et al.* [19]	Presented joint channel estimators and multi-user detectors relying on the RWBS, the GA, the PSO and the DE algorithms, comparing their performance and complexity.
2015	Prasad *et al.* [15]	Presented a joint channel estimator and data detector requiring fewer pilot symbols, by exploiting the sparsity of the wireless channel.

estimator and multi-user detector. We then compare it to a system, where either the optimal Maximum A posteriori Probability (MAP) MUD or the RWBS-aided CE are employed, demonstrating that the quantum-assisted joint CE and MUD achieve both a better performance and lower complexity. We evaluate our quantum-assisted algorithm's performance with the aid of the CE MSE curves, as well as BER plots, while comparing it to systems, where perfect channel estimation is available. We characterise the performance of rank-deficient scenarios, of Channel Impulse Response (CIR) prediction filters, the effects of the channels' Power Delay Profile (PDP) and of the Doppler frequency on the proposed algorithm's performance and complexity.

3) *We also suggest a modification for the weighted boosting search component of the RWBS and subsequently of the QRWBS and then analyse the associated performance improvement.*

The paper is structured as described in Fig. 1. In Section II we present the SDMA-OFDM system's model, including the pilot-assisted channel estimation, the CIR prediction filter, as well as the joint MUD and CE operations. In Section III the iterative processes of the MUD, of the CE and of the decoders are detailed. In Section IV a rudimentary introduction to quantum computing is provided, along with the quantum algorithms that will be employed by our QRWBS. Furthermore, in Section V we design the QRWBS and compare its algorithmic steps to those of the RWBS, while in Section VI their complexity is quantified. Moreover, in Section VII we employ the QRWBS-aided CE in the context of various MIMO-OFDM systems and evaluate its performance both with the aid of the CE MSE and the system's BER. Finally, our conclusions are offered in Section VIII.

II. SYSTEM MODEL

Let us consider the uplink of an SDMA-OFDM system [2], where the uth user, $u = 1, 2, \ldots, U$, initially encodes his/her information bits $\{b_u\}$ using a turbo channel encoder, as illustrated in Fig. 2. The resultant encoded bits $\{c_u\}$ are then interleaved and mapped to M-ary symbols $\{x_u\}$. The same interleaving sequence is used for each user. The symbols are converted from a single serial stream to W parallel streams, where W is the number of subcarriers that each user will transmit in, out of Q available subcarriers. Let us assume the worst-case scenario, which leads to the maximum possible Multi-User Interference (MUI), where each user always transmits on all the available subcarriers, leading to $W = Q$. Each parallel stream is then modulated by using a Q-point Inverse Fast Fourier Transform (IFFT) and the Q modulated symbols are transmitted over the wireless Rayleigh fading channel.

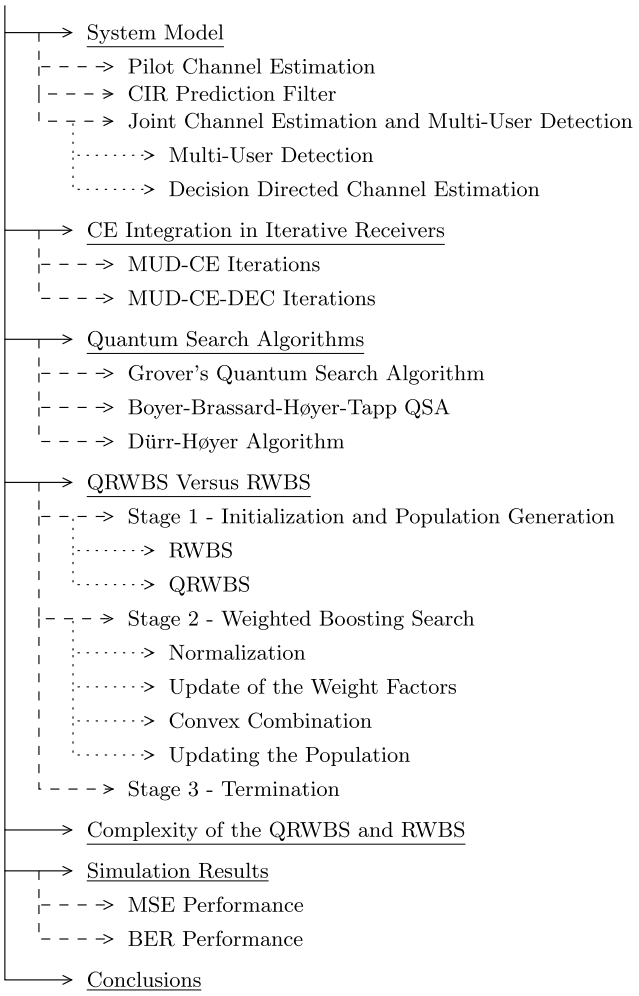

FIGURE 1. Summary of the sections of the paper.

The P receive AEs of the BS receive the U faded transmitted signals. Let us consider a synchronous system, where the U transmitted signals arrive simultaneously to the P receive AEs, therefore they are added together at each receive AE, along with the Additive White Gaussian Noise (AWGN), which is a random, Gaussian-distributed, complex-valued variable with a zero mean and a variance of $N_0 = 2\sigma^2$. The proposed joint quantum-assisted channel estimator and multi-user detector is expected to be able to work in the presence of both time and/or frequency synchronization mismatch, by suitably changing the search space of the quantum search algorithms. In more detail, the QMUD would search for the most probable multi-level symbol in more than one delay taps and more than one subcarrier simultaneously, by allowing a legitimate multi-level symbol to take a different form, where a user's symbol may have been received in all probable time and/or frequency resources. This would increase the number of legitimate multi-level symbols and hence the complexity of both the full search and of the quantum search algorithms. Time synchronization may also be achieved with the use of midambles. This would also result in requiring a lower complexity in the joint channel estimator and multi-user detector, when the midamble is included in different parts of a user's transmission burst during a time slot. Furthermore, it would allow a detection of the number of users U supported by the system, when this number is not known *a priori* at the BS. In any case, since the process would remain a search problem, the quantum search algorithms are still expected to require a lower complexity than the full search.

Focusing on the qth subcarrier of the oth OFDM symbol, the received signal at the BS is

$$\mathbf{y}_{o,q} = \mathbf{H}_{o,q} \cdot \mathbf{x}_{o,q} + \mathbf{n}_{o,q}, \tag{1}$$

where $\mathbf{y}_{o,q} = [y_{1,o,q}, y_{2,o,q}, \ldots, y_{P,o,q}]^T$ is the $(P\times 1)$-element received signal vector and $\mathbf{H}_{o,q}$ is the Frequency-Domain CHannel Transfer Function (FD-CHTF) on the qth subcarrier of the oth OFDM symbol, which may be represented by a $(P\times U)$-element matrix as in

$$\mathbf{H}_{o,q} = \begin{bmatrix} H^{(1)}_{1,o,q} & H^{(2)}_{1,o,q} & \cdots & H^{(U)}_{1,o,q} \\ H^{(1)}_{2,o,q} & H^{(2)}_{2,o,q} & \cdots & H^{(U)}_{2,o,q} \\ \vdots & \vdots & \ddots & \vdots \\ H^{(1)}_{P,o,q} & H^{(2)}_{P,o,q} & \cdots & H^{(U)}_{P,o,q} \end{bmatrix}, \tag{2}$$

where $H^{(u)}_{p,o,q}$ is the complex-valued channel coefficient between the uth user and the pth receive AE on the qth subcarrier of the oth OFDM symbol. Moreover, still referring to (1), $\mathbf{x}_{o,q} = [x^{(1)}_{o,q}, x^{(2)}_{o,q}, \ldots, x^{(U)}_{o,q}]^T$ is the $(U\times 1)$-element symbol vector of the U users on the qth subcarrier of the oth OFDM symbol and $\mathbf{n}_{o,q} = [n_{1,o,q}, n_{2,o,q}, \ldots, n_{P,o,q}]^T$ is the $(P\times 1)$-element noise vector.

The FD-CHTF coefficients between the uth user and the pth receive AE are generated by the Q-point Fast Fourier Transform (FFT) of the time-domain CIR $\mathbf{h}^{(u)}_{p,o}$ for the oth OFDM symbol, where

$$\mathbf{h}^{(u)}_{p,o} = \left[h^{(u)}_{p,o,1}, h^{(u)}_{p,o,2}, \ldots, h^{(u)}_{p,o,L}\right]^T. \tag{3}$$

In (3), $h^{(u)}_{p,o,l}$ is the Rayleigh-distributed complex-valued time-domain channel coefficient of the lth multipath delay tap, $l = 1, 2, \ldots, L$, of the channel between the uth user and the pth receive AE during the oth OFDM symbol and L is the index of the channel's last delay tap. In this paper we have assumed that each channel has a time-invariant CIR, therefore the specific delay tap indices of each channel remain unaltered for all the transmitted OFDM symbols, as encapsulated in $L[o] = L$. On the other hand, the channel of each delay path is independently fading following the Rayleigh distribution and having a normalized Doppler frequency of f_d, as in $\mathbf{h}^{(u)}_{p,o} \neq \mathbf{h}^{(u)}_{p,o-1}$. Let us emphasize that L is not the number of paths of a channel, but the index of the last delay tap of a channel. More importantly, we do not assume any knowledge about the number of paths of a channel. For example, in a scenario, where a channel's power delay profile consists of 4 paths, according to which the first three paths are represented by the first three CIR taps and the last path arrives at

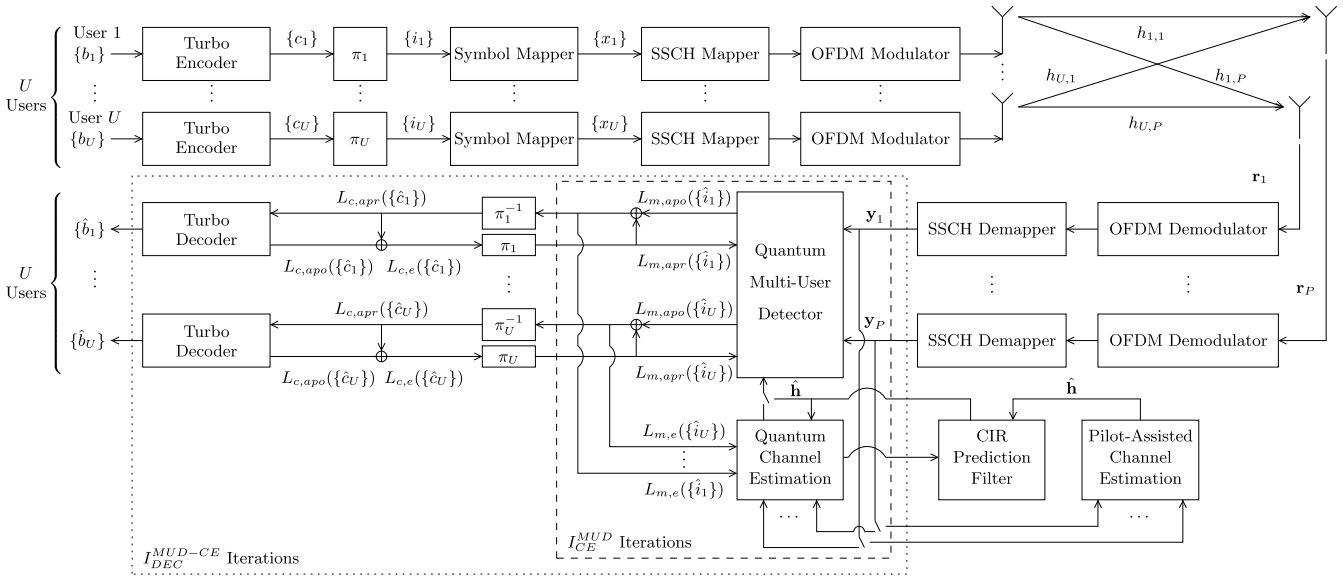

FIGURE 2. SDMA-OFDM uplink communication system's block diagram supporting *U* users employing Turbo coding as well as iterative, joint Quantum-assited CE and soft-input soft-output QMUD at the BS.

the 20th delay tap, we have $L = 20$, without assuming any knowledge about the total number of paths. Based on (3), we may obtain the FD-CHTF between the uth user and the pth receive AE during the oth OFDM symbol as in [17]

$$\mathbf{H}_{p,o}^{(u)} = \mathbf{F}_{Q,L} \cdot \mathbf{h}_{p,o}^{(u)}, \tag{4}$$

where

$$\mathbf{H}_{p,o}^{(u)} = \left[H_{p,o,1}^{(u)}, H_{p,o,2}^{(u)}, \ldots, H_{p,o,Q}^{(u)}\right]^T \tag{5}$$

is the Q-element FD-CHTF vector and $\mathbf{F}_{Q,L}$ is the $(Q \times L)$-element FFT matrix, which may be obtained by taking the first L columns of the $(Q \times Q)$-element FFT matrix $\mathbf{F}_{Q,Q}$, where $F_{q,l} = \exp\left[-j2\pi(q-1)(l-1)/Q\right]$ with $q = 1, 2, \ldots, Q$ and $l = 1, 2, \ldots, L$.

In this contribution, we have adopted the assumption of all users having the same Doppler frequency, for achieving homogeneity and fairness between the users' performance. For the same reasons, we opted for all multi-path channels to have the same number of delay paths L. In practice, when the multi-path channels between a user and a receive antenna element have different number of paths, L will be a function of u and p. Please note that the proposed joint quantum-assisted channel estimation and multi-user detection algorithm will not differ in those scenarios, but the performance of each user would be unique. Furthermore, all receive antenna elements and all users are assumed to be sufficiently separated in space, so that there is no spatial correlation between two channels. Nevertheless, if spatial correlation was present, the proposed algorithm would still operate normally. However, the performance of any classical or quantum-assisted algorithm performing joint channel estimation and multi-user detection would be degraded, since spatial correlation at the receive antenna elements would lower the diversity order and spatial correlation between two users' antennas would increase their multi-user interference.

A. PILOT CHANNEL ESTIMATION

Channel estimation is performed for obtaining the channel coefficients of each OFDM symbol. More specifically, starting from the first OFDM symbol and every Δ_t OFDM symbols, an OFDM symbol is transmitted by each user with user-specific pilot symbols transmitted on each subcarrier [18], resulting in a preamble arrangement of the training symbols. Please note that the proposed joint channel estimation and multi-user detection algorithm may also be used in systems, where a scattered pilot arrangement is adopted, by suitably adjusting the pilot-based channel estimation and prediction. All the pilot symbols are assumed to be known at the BS. The difference with respect to the pilot symbols in [18] is that in our scenarios the signals are not assumed to be separated with the aid of orthogonal spreading codes on each subcarrier, but rather only in the spatial domain. By doing this, we may allow the MUI to contaminate in the CE, but the required bandwidth is smaller and the transmission process remains the same as that of the subsequent OFDM symbols. Let us distinguish the symbols as data OFDM symbols and pilot OFDM symbols, depending on whether information symbols or pilot symbols are transmitted on each of their subcarriers, respectively. The user-specific pilot symbol sequence may either be random, or optimized with respect to the number of users U and the number of subcarriers Q [4], for achieving the lowest possible MUI.

The CE relying on a pilot OFDM symbol is performed in the time domain, by using the Least Squares (LS) channel estimator on a per receive AE basis [1], [17], [19], since each AE has received a unique signal, where the pilot signals are

superimposed and contaminated by the AWGN. Therefore, based solely on the received signal at the pth receive AE, the employment of the LS CE yields an $(L \times U)$-element complex-valued vector with the CIRs of the channels between all U users and the pth receive AE described as

$$\hat{\mathbf{h}}_{p,o} = \left[\hat{\mathbf{h}}_{p,o}^{(1)T}, \hat{\mathbf{h}}_{p,o}^{(2)T}, \hat{\mathbf{h}}_{p,o}^{(U)T}\right]^T, \quad (6)$$

where $\hat{\mathbf{h}}_{p,o}^{(u)}$ is the estimate of $\mathbf{h}_{p,o}^{(u)}$, which is given in (3).

The reason we opted for a time domain CE performed on a per receive AE basis instead of a frequency domain CE performed on a per subcarrier basis is the exploitation of the correlation between the frequency domain samples of a channel due to the FFT, which is acquired during a time domain CE, but ignored during a frequency domain CE. Furthermore, we opted for estimating the CIR of each channel instead of straightforwardly estimating its FD-CHTF due to the fact that $(L \times U)$ variables have to be estimated in the CIR CE scenario, in contrast to $(Q \times U)$ variables for the latter case. In practice we have $L < Q$, hence we have to estimate fewer continuous, complex-valued variables if we aim for estimating the CIRs instead of the FD-CHTFs. Please note that in our system the symbols transmitted by multiple users on the same subcarrier may only be separated in the spatial domain.

B. CIR PREDICTION FILTER

As illustrated in Fig. 2, before the initial MUD on every data OFDM symbol, the CIR prediction filter [1] is employed for providing a better initial CIR estimate $\hat{\mathbf{h}}_{pr,p,o}$, where

$$\hat{\mathbf{h}}_{pr,p,o} = \left[\hat{\mathbf{h}}_{pr,p,o}^{(1)T}, \hat{\mathbf{h}}_{pr,p,o}^{(2)T}, \hat{\mathbf{h}}_{pr,p,o}^{(U)T}\right]^T, \quad (7)$$

and $\hat{\mathbf{h}}_{pr,p,o}^{(u)}$ is the predicted CIR during the oth OFDM symbol of the channel between the uth user and the pth receive AE. The CIR prediction filter is based on the estimated CIRs of the N_{tap} previous OFDM symbols, $\hat{\mathbf{h}}_{p,o-1}, \ldots, \hat{\mathbf{h}}_{p,o-N_{tap}}$, the number of subcarriers Q, the normalized effective Doppler frequency $F_d = Q \cdot f_d$, the modulation scheme, the number of users U, the index of the last delay path L of the channel's power delay profile and the noise power N_0. The prediction filter's order is equal to N_{tap}. During each use of the CIR prediction filter, the filter's coefficients have to be estimated.

It is expected that a filter with a higher order will provide a better initial CIR estimate, since it will depend on more CIRs related to past OFDM symbols. Since we assume that all the users experience the same Doppler frequency and they use the same modulation scheme, the same filter coefficients will be used by all the users [1]. In addition, the same filter coefficients will be used for predicting the channel on each of the L delay paths.

C. JOINT CHANNEL ESTIMATION AND MULTI-USER DETECTION

The CIRs of Section II-B, predicted during a data OFDM symbol are used for performing MUD during the same data OFDM symbol. More specifically, having obtained $\hat{\mathbf{h}}_{pr,p,o}^{(u)}$ for $u = 1, 2, \ldots, U$, $p = 1, 2, \ldots, P$, we initially assume

$$\hat{\mathbf{h}}_{p,o}^{(u)} = \hat{\mathbf{h}}_{pr,p,o}^{(u)}, \quad (8)$$

where $\hat{\mathbf{h}}_{p,o}^{(u)}$ is described in (6), and we may calculate $\hat{\mathbf{H}}_{p,o}^{(u)}$ based on (4), finally resulting in an estimate of the FD-CHTF on the qth subcarrier $\hat{\mathbf{H}}_{o,q}$, by combining (2) and (5). Therefore, starting from the FD-CHTF predicted for the current OFDM symbol based on the previous OFDM symbols, we perform Joint Channel Estimation and Multi-User Detection (JCEMUD) [11], [17]–[19].

Firstly, we perform MUD on a per subcarrier basis, assuming the initially estimated FD-CHTF to be $\hat{\mathbf{H}}_{o,q}$ for each subcarrier. Please note that the initially estimated FD-CHTF is predicted based on the previous OFDM symbols, therefore it may differ significantly from the actual FD-CHTF of (2) if the effective Doppler frequency $F_d = Q \cdot f_d$, which is the Doppler frequency that each subcarrier effectively experiences from one OFDM symbol to the next, is too high, or the prediction filter order N_{tap} is not sufficiently high. We will demonstrate that we may obtain erroneous initial symbol estimates by the MUD even in noiseless scenarios, if F_d is too high in association with a low prediction filter order N_{tap}, since the initial channel estimates generated during the previous OFDM symbol have low correlation with the actual ones in the current OFDM symbol. The MUD may provide soft or hard outputs, and it may receive soft inputs from the channel decoder in the form of *a priori* LLRs. The performance is expected to be improved when a SISO MUD is employed. In this treatise we will investigate the employment of a SISO QMUD.

Having obtained the symbol estimates $\mathbf{x}_{o,q}$ for each subcarrier q of the oth OFDM symbol, we use them in DDCE [1], [17], [19], with the aid of the proposed quantum-assisted repeated weighted boosting search.

1) MULTI-USER DETECTION

The MUD is performed on a per subcarrier basis, therefore the Cost Function (CF) may be described as [2], [30], [32]

$$f_{MUD}\left(\hat{\mathbf{H}}_{o,q}, \mathbf{x}_{o,q}\right) = \exp\left(-\frac{\left\|\mathbf{y}_{o,q} - \hat{\mathbf{H}}_{o,q} \cdot \mathbf{x}_{o,q}\right\|^2}{N_0}\right) P(\mathbf{x}_{o,q}), \quad (9)$$

where $P(\mathbf{x}_{o,q})$ is the *a priori* symbol probability of the multi-level symbol $\mathbf{x}_{o,q}$, which is fed back to the MUD from the channel decoders of Fig. 2. Initially we assume that $P(\mathbf{x}_{o,q}) = M^{-U}$, for all legitimate $\mathbf{x}_{o,q}$. A HIHO MUD finds the specific symbol vector $\hat{\mathbf{x}}_{o,q,\max}$ that maximizes the CF f_{MUD} of (9), as in

$$\hat{\mathbf{x}}_{o,q,\max} = \underset{\mathbf{x}_{o,q} \in \mathcal{M}^U}{\arg\max} \left\{ f_{MUD}\left(\hat{\mathbf{H}}_{o,q}, \mathbf{x}_{o,q}\right) \right\}. \quad (10)$$

On the other hand, a SISO MUD estimates the bit-based *a posteriori* Log Likelihood Ratios (LLR) of the multi-user

symbol, as encapsulated in [2], [7], [30], [32]

$$L_{m,po}\left(b_u^{(m)}\right) = \ln \frac{\sum_{\mathbf{x}\in\chi(u,m,0)} f_{MUD}\left(\hat{\mathbf{H}}_{o,q}, \mathbf{x}_{o,q}\right)}{\sum_{\mathbf{x}\in\chi(u,m,1)} f_{MUD}\left(\hat{\mathbf{H}}_{o,q}, \mathbf{x}_{o,q}\right)}, \quad (11)$$

where $L_{m,po}\left(b_u^{(m)}\right)$ is the *a posteriori* LLR of the uth user's mth bit and $\chi(u, m, \mathrm{v})$ is the subset of legitimate symbols that have the uth user's mth bit equal to v.

Regardless of the specific nature of the selected MUD, a hard decision is made on the output of the MUD and the resultant symbol is forwarded to the DDCE. The CE will be based on the symbols detected on all the subcarriers of the oth OFDM symbol and it will provide an improved estimate of the FD-CHTF, which may in turn be exploited by the MUD of the current OFDM symbol for detecting a more reliable multi-level symbol, or by the MUD of the $(o+1)$th OFDM symbol, which will use it as its initial channel estimate, in the same way as the oth OFDM symbol initially used the FD-CHTF estimated during the $(o-1)$th OFDM symbol.

Still referring to the oth OFDM symbol, after a predetermined number of I_{CE}^{MUD} iterations between the MUD and the CE [11], [19], the resultant hard estimates in the case of a HIHO MUD, or the extrinsic LLRs, which are obtained by the *a posteriori* LLRs of (11) based on

$$L_{m,e}\left(b_u^{(m)}\right) = L_{m,po}\left(b_u^{(m)}\right) - \ln \frac{P\left(b_u^{(m)}=0\right)}{P\left(b_u^{(m)}=1\right)}, \quad (12)$$

are deinterleaved and forwarded to the channel decoders as *a priori* LLRs. Following the decoding procedure, the extrinsic LLRs at the output of the channel decoders may be fed back to the MUD after the interleaving procedure for aiding it to provide a better symbol estimate. After I_{DEC}^{MUD-CE} iterations between the JCEMUD and the decoders of Fig. 2, a hard decision is performed at the extrinsic LLRs at the output of the decoders, providing us with the estimated information bits $\{\hat{b}_u\}$, for $u = 1, 2, \ldots, U$.

2) DECISION DIRECTED CHANNEL ESTIMATION

The DDCE is performed on a per receive AE basis by allowing the hard decision at the output of the MUD to direct and guide the search for finding the CIR that minimizes the MSE between the received signals on each subcarrier of a receive AE and the corresponding detected symbols at the output of the MUD [1], [17], [19]. Hence, the CF of the DDCE may be defined as

$$f_{CE}\left(\mathbf{h}_{p,o}, \hat{\mathbf{X}}_o\right) = \left\| \mathbf{Y}_{p,o} - \hat{\mathbf{X}}_o^T \cdot \mathbf{F}_{Q,L} \cdot \mathbf{h}_{p,o} \right\|^2, \quad (13)$$

where $\mathbf{h}_{p,o}$ is the $(UL \times 1)$-element CIR vector described in (6), $\hat{\mathbf{X}}_o$ is a $(UQ \times Q)$-element matrix constructed by the detected symbols at the MUD as in

$$\hat{\mathbf{X}}_o = \left[\hat{\mathbf{X}}_o^{(1)}, \hat{\mathbf{X}}_o^{(2)}, \ldots, \hat{\mathbf{X}}_o^{(U)}\right]^T, \quad (14)$$

$$\hat{\mathbf{X}}_o^{(u)} = \mathrm{diag}\left\{\hat{x}_{o,1}^{(u)}, \hat{x}_{o,2}^{(u)}, \ldots, \hat{x}_{o,Q}^{(u)}\right\}, \quad (15)$$

$\mathbf{Y}_{p,o}$ is the $(Q \times 1)$-element vector, which contains the signals received on the Q subcarriers at the pth receive AE as in

$$\mathbf{Y}_{p,o} = \left[y_{p,o,1}, y_{p,o,2}, \ldots, y_{p,o,Q}\right]^T, \quad (16)$$

and $\mathbf{F}_{Q,L}$ is the FFT matrix as stated in Section II.

The output of the DDCE is the specific $\mathbf{h}_{p,o,\min}$ that satisfies

$$\mathbf{h}_{p,o,\min} = \arg\min_{\mathbf{h}_{p,o}\in\mathbb{C}^{UL}} \{f_{CE}\}. \quad (17)$$

The CIR of (17) estimated at each receive AE is used by the MUD of Section II-C1 of the current oth OFDM symbol, if further MUD-CE iterations are allowed, or as an input CIR in the CIR prediction filter of the subsequent, $(o+1)$th OFDM symbol. In this paper, we propose the QRWBS algorithm for performing fast and accurate DDCE.

III. CE INTEGRATION IN ITERATIVE RECEIVERS

As illustrated in Fig. 2 and briefly stated in Section II, the CE process may be integrated in receivers, where iterations are allowed between the MUD, the CE and the DEC processing blocks. More specifically, in our systems iterations may be performed between the MUD and the CE, as well as between the MUD, the CE and the decoders.

A. MUD-CE ITERATIONS

In our scenario, I_{CE}^{MUD} number of iterations may be allowed between the MUD and the CE before the information at the output of the MUD is passed to the decoders. In more detail, the initial MUD process on an OFDM symbol is performed on a per subcarrier basis during the $i_{CE}^{MUD} = 1$st MUD-CE iteration, relying on the predicted channel estimates of the current OFDM symbol's CIR prediction filter. After determining the detected symbol, the CE is taking over on a per receive AE basis, for updating the CIR, which corresponds to a low MSE in (13). During the $i_{CE}^{MUD} = 2$nd MUD-CE iteration, the MUD is activated again for detecting a multi-level symbol on each subcarrier, by using the updated channel estimates.

After I_{CE}^{MUD} iterations, the extrinsic LLRs at the output of the MUD are fed to the U channel decoders. It should be mentioned that the CE is also performed at the I_{CE}^{MUD}th iteration, even though the channel decoders will use the extrinsic LLRs of the MUD, which were calculated based on the CIRs estimated during the $(I_{CE}^{MUD}-1)$th iteration. The reason for performing the CE even during the last MUD-CE iteration is that these updated channel estimates will be used by the CIR prediction filter of the next OFDM symbol. However, they may also be used for the current OFDM symbol, when iterations are allowed between the MUD and the decoders, as analysed in Section III-B.

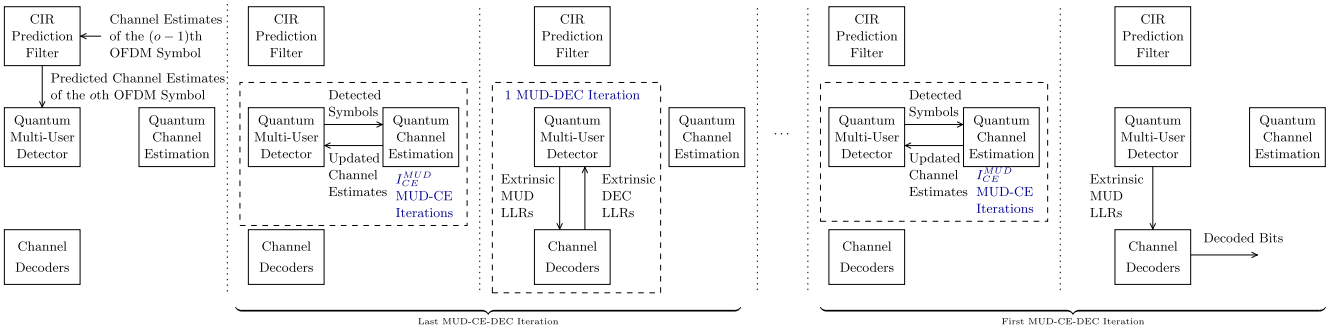

FIGURE 3. The sequence of block activations at the base station, as well as the I_{CE}^{MUD} and I_{DEC}^{MUD-CE} iterations.

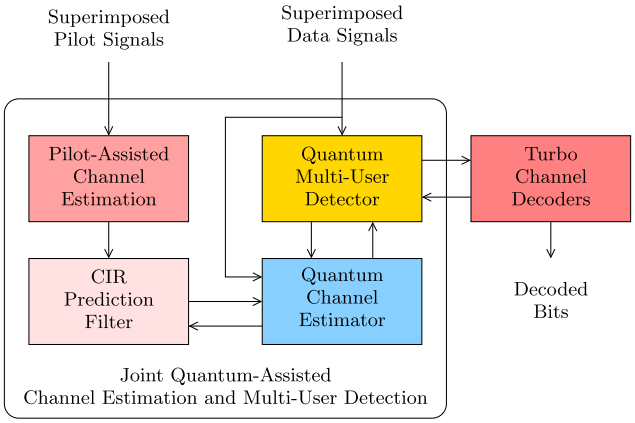

FIGURE 4. Abstract system model of an uplink receiver in a Non-Orthogonal Multiple Access (NOMA) system, employing Joint Quantum-assisted Channel Estimation and Multi-User Detection.

B. MUD-CE-DEC ITERATIONS

As described in Fig. 3, before the $i_{DEC}^{MUD-CE} = 1$st MUD-CE-Decoders (DEC) iteration, the initial channel estimates used in the MUD of an OFDM symbol are the ones estimated by the CIR prediction filter of the current OFDM symbol. During the i_{DEC}^{MUD-CE}th MUD-CE-DEC iteration, with $i_{DEC}^{MUD-CE} > 1$, the CIRs used by the MUD during the $i_{CE}^{MUD} = 1$st MUD-CE iteration are the ones estimated during the last MUD-CE iteration of the previous, $(i_{DEC}^{MUD-CE} - 1)$th, MUD-CE-DEC iteration. Therefore, the channel estimates are not only saved for use by the CIR prediction filters of the subsequent OFDM symbols, but also for subsequent MUD-CE-DEC iterations of the current OFDM symbols. The reason for opting for this methodology is that the estimated CIRs during the previous MUD-CE-DEC iteration for the oth OFDM symbol are expected to offer a lower MSE than the predicted CIRs of the same OFDM symbol, since they have been estimated for that specific OFDM symbol, having already closed the remaining gap created by the effective normalized Doppler frequency F_d and the AWGN, as well as having already taken into consideration the previous *a priori* LLRs provided by the channel decoders of Fig. 2 for the oth OFDM symbol. An abstract version of the block activations and information exchange is summarized in Fig. 4.

IV. QUANTUM SEARCH ALGORITHMS

Quantum computing employs quantum bits or *qubits*.[1] In contrast to a classical bit, which may assume the values 0 or 1, a qubit $|q\rangle$ may be in a superposition of these two states, as in

$$|q\rangle = \alpha|0\rangle + \beta|1\rangle, \tag{18}$$

where $|\alpha|^2$ and $|\beta|^2$ are the probabilities of observing the qubit in the $|0\rangle$ and $|1\rangle$ states, respectively, with $\alpha, \beta \in \mathbb{C}$ and $|\alpha|^2 + |\beta|^2 = 1$. When a so-called measurement or observation is performed on a qubit, its state collapses to one of the measurement's bases. In the investigated QSAs, the measurement basis employed is the computational basis $\{|0\rangle, |1\rangle\}$ [21]–[23].

Quantum registers may be formed by using more than one qubits. The qubits may be independent, or *entangled* [21]–[23]. For example, a quantum register $|q_1\rangle|q_2\rangle = (|00\rangle + |01\rangle)/\sqrt{2} = |0\rangle(|0\rangle + |1\rangle)/\sqrt{2}$ includes the two independent qubits $|q_1\rangle = |0\rangle$ and $|q_2\rangle = (|0\rangle + |1\rangle)/\sqrt{2}$, since observing any of them does not affect the quantum state of the other one. However, a quantum register associated with $|\phi_1\rangle|\phi_2\rangle = (|00\rangle + |11\rangle)/\sqrt{2}$ includes two entangled qubits, since the individual qubits cannot be represented separately and measuring one affects the state of the other.

The quantum states of the qubits are evolved by using unitary operators, such as the Hadamard operator H [21]–[23], which creates an equiprobable superposition of the computational basis states, as in $|+\rangle = H|0\rangle = (|0\rangle + |1\rangle)/\sqrt{2}$ and $|-\rangle = H|1\rangle = (|0\rangle - |1\rangle)/\sqrt{2}$.

In the analysis of the following QSAs and their applications, we only use real-valued amplitudes α and β for a qubit's states. Furthermore, when a decimal number appears in a *ket* $|\cdot\rangle$, that number is the decimal representation of the binary string created by the quantum register's qubits. For instance, we have $|5\rangle = |101\rangle = |1\rangle|0\rangle|1\rangle$.

A. GROVER'S QUANTUM SEARCH ALGORITHM

The average complexity, quantified in terms of the average number of Cost Function Evaluations (CFE), for searching

[1]For an extensive tutorial on quantum computing and quantum search algorithms, please refer to [7].

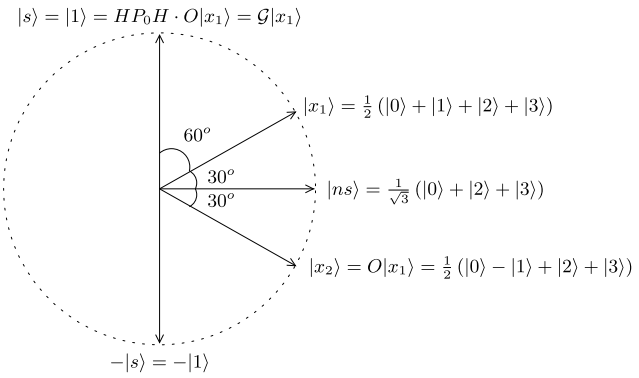

FIGURE 5. Example of Grover's QSA in a database with $N = 4$ entries and $S = 1$ solution. The solution state is $|1\rangle$.

with classical computing for the index x_s which leads to $f(x_s) = \delta$ for a desired value δ and function f with N legitimate entries is $O(N/S)$, where S is the number of different indices that have the same output δ, also termed as *solutions*. By contrast, Grover's QSA is able to find the index $|x_s\rangle$ that corresponds to $f(x_s) = \delta$ with as few as $O(\sqrt{N/S})$ CFEs [24], [25].

Grover's QSA initially creates an equiprobable superposition of all N legitimate states, as in

$$|x\rangle = \frac{1}{\sqrt{N}} \sum_{x=0}^{N-1} |x\rangle, \tag{19}$$

by using $n = \log_2(N)$ qubits. Afterwards, the Grover operator [24]

$$\mathcal{G} = HP_0H \cdot O \tag{20}$$

is applied L_{opt} number of times to the initial quantum state of (19), where H is the Hadamard operator, P_0 is a unitary operator that evolves $|x\rangle$ to $-|x\rangle$ if and only if $|x\rangle = |0\rangle$, O is a unitary operator termed as the *Oracle* [25], which evolves $|x\rangle$ to $-|x\rangle$, when $f(x) = \delta$, and L_{opt} is equal to

$$L_{opt} = \left\lfloor \pi/4\sqrt{N/S} \right\rfloor. \tag{21}$$

The Oracle evaluates the function f for all superimposed quantum states and marks the specific solution indices x_s, which satisfy $f(x_s) = \delta$, by flipping their quantum state's sign. By doing so, when the resultant quantum state $|x'\rangle = \mathcal{G}^{L_{opt}}|x\rangle$ is observed, there is an $\sim$100% success probability of obtaining a state $|x_s\rangle$ that satisfies $f(x_s) = \delta$. In order for Grover's QSA to be employed, the specific value δ, as well as the number of solutions S and the number of legitimate inputs N have to be known *a priori*.

Figure 5 presents an example, when Grover's QSA is employed in a database with $N = 4$ entries and there is $S = 1$ solution. In our example, the state $|1\rangle$ is the solution, therefore, Grover's QSA will be successful if it eventually observes that state. Initially, we create an equiprobable superposition of states, $|x_1\rangle = \frac{1}{2}(|0\rangle + |1\rangle + |2\rangle + |3\rangle)$. In Fig. 5 we have plotted $|x_1\rangle$ with respect to the orthogonal quantum states $|s\rangle = |1\rangle$, which represents the solution state and $|ns\rangle = \frac{1}{\sqrt{3}}(|0\rangle + |2\rangle + |3\rangle)$, which represents the equiprobable superposition of states that are not solutions. The angle between $|x_1\rangle$ and $|ns\rangle$ is equal to $\arcsin\left(\sqrt{S/N}\right) = 30^o$. After the application of the Oracle, the solution state is reflected with respect to the quantum state $|ns\rangle$, since the Oracle only flips the sign of the solution state $|1\rangle$. Afterwards, the diffusion operator $D = HP_0H$ reflects the state $|x_2\rangle$ with respect to the initial superposition of states $|x_1\rangle$, resulting in the state $\mathcal{G}|x_1\rangle = |s\rangle = |1\rangle$. Since $L_{opt} = 1$ according to (21), we stop here and observe the resultant state. Since $\mathcal{G}|x_1\rangle = |1\rangle$, we will observe the solution state with certainty. It should be noted that if $N/S \neq 4$, the optimal resultant state $\mathcal{G}^{L_{opt}}|x_1\rangle$ after L_{opt} Grover iterations will not be equal to $|s\rangle$, but very close to it. This is the reason why Grover's QSA has a $\sim$100% probability of success.

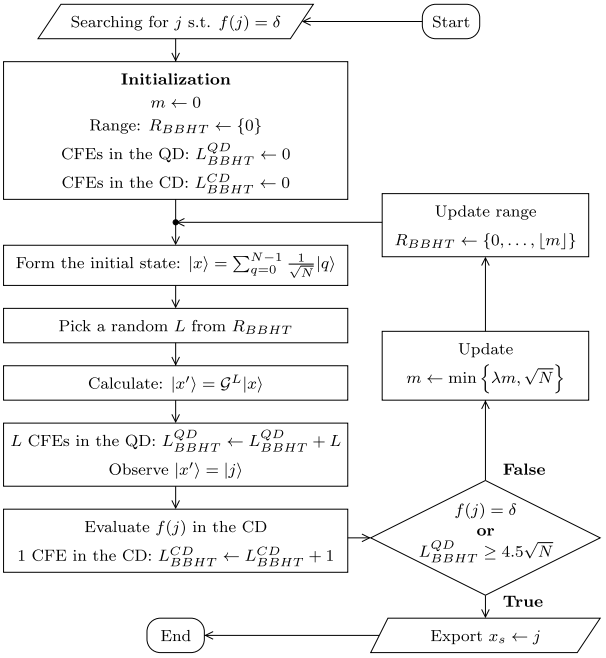

FIGURE 6. Flow chart of the BBHT QSA [32].

B. BOYER-BRASSARD-HØYER-TAPP QSA

When the number of solutions S is not known, but δ and N are available, a variant of Grover's QSA, namely the BBHT QSA [26] may be used. The BBHT QSA uses the Grover operator $\mathcal{G}$ of Section IV-A, but since L_{opt} of (21) cannot be calculated due to the uncertainty of S, the Grover operator $\mathcal{G}$ is applied to the initial state a pseudo-random number of times. After observing the resultant quantum state, it is verified whether a solution $|x_s\rangle$ was obtained or not. If not, the Grover operator is applied again to the initial state of (19) another pseudo-random number of times, as seen in the flowchart of Fig. 6 [32]. It was proved in [26] that the BBHT QSA finds a solution $|x_s\rangle$ after $O(\sqrt{N/S})$ CFEs with a $\sim$ 100% success probability. If no solution has been observed during

the BBHT QSA after $4.5\sqrt{N}$ CFEs in the quantum domain, it is concluded that there are no solutions.

C. DÜRR-HØYER ALGORITHM

When both the number of solutions S and the value δ are unavailable, then neither the BBHT QSA nor Grover's QSA may be used. If, however, a known desired attribute of the searched value is available, alternate QSAs may be employed. For example, if the specific $x_{\min}$ that minimizes the function $f(x_{\min}) \leq f(x)$, for all legitimate x, has to be found, but the specific $\delta = f(x_{\min})$ is not available, the DHA [27] may be used. The DHA succeeds in finding $x_{\min}$ after $O(\sqrt{N})$ CFEs with $\sim$100% success probability.

The DHA is initialized by using the CF value of either a random index [27], or of a carefully selected index x_i [29]. The DHA then applies a unitary operator to the equiprobable quantum state of (19) a pseudo-random number of times with the aim of finding an index x_s that has a lower CF value than the index x_i, as encapsulated in

$$f(x_s) < f(x_i). \tag{22}$$

Grover's operator of (20) with an alternate Oracle O_{DHA} is applied a pseudo-random number of times, because the number of indices S that satisfy (22) is unavailable and L_{opt} of (21) cannot be calculated. More specifically, DHA's Oracle O_{DHA} marks as solutions the specific states $|x_s\rangle$ that satisfy $f(x_s) < f(x_i)$ by flipping their quantum state's sign. Once a solution x_s is found, that specific state becomes $x_i = x_s$, its CF value becomes the new $\delta = f(x_i) = f(x_s)$ and the process restarts. If no solution has been found after $4.5\sqrt{N}$ CFEs following the last update of δ, it is concluded that we have $x_{\min} = x_i$ and the DHA stops. As investigated in [30], the DHA starts from an initial state and finally finds $x_{\min}$ by evaluating the CF for continuously "better" indices x during its operation. The flow chart of the DHA is presented in Fig. 7 [32].

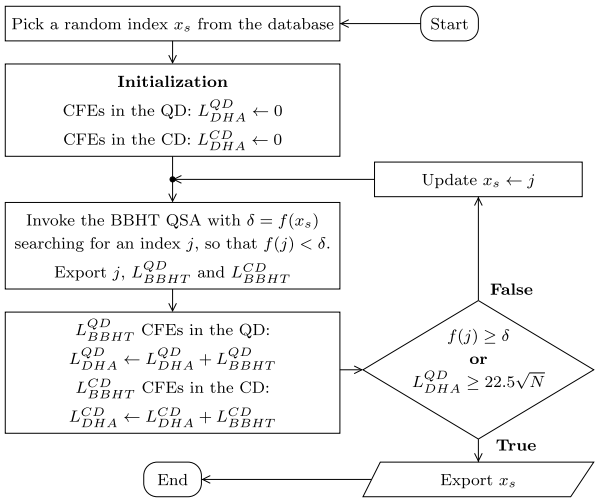

FIGURE 7. Flow chart of the DHA [32].

Algorithm 1 Repeated Weighted Boosting Search for Channel Estimation

1: Set $\mathbf{h}_{\text{best},0} \leftarrow \mathbf{h}_{p,o-1,\min}, f_{\text{best},0} \leftarrow f_{CE}\left(\mathbf{h}_{p,o-1,\min}, \hat{\mathbf{X}}_o\right)$.
2: Set $\xi \leftarrow 1$.
3: **while** $\xi \leqslant \Xi$ AND $f_{\text{best},\xi-1} - f_{\text{best},\xi} > \Delta_\Xi$ **do**
4: Let $\mathbf{h}_{\xi,1} \leftarrow \mathbf{h}_{\text{best},\xi-1}$ be the first individual of the ξth generation.
5: Create $Z-1$ individuals, $\mathbf{h}_{\xi,\zeta}$, $\zeta = 2, 3, \ldots, Z$, based on $\mathbf{h}_{\text{best},\xi-1}$ and according to (23).
6: Evaluate the CE CF of (13) for those $Z-1$ individuals.
7: Update $\mathbf{h}_{\text{best},\xi}$ based on (24), along with $f_{\text{best},\xi}$.
8: Update $\mathbf{h}_{\text{worst},\xi}$, $\mathbf{h}_{\text{2nd worst},\xi}$ based on (25) and (26), respectively, along with $f_{\text{worst},\xi}$ and $f_{\text{2nd worst},\xi}$.
9: Set the weight factors $\delta^{(1)}_{\xi,\zeta}$ to $1/Z$ for all $\zeta = 1, 2, \ldots, Z$.
10: **for** $t_{WBS} = 1, 2, \ldots, T_{WBS}$ **do**
11: Normalize the CF values based on (28).
12: Calculate the weight factors $\delta^{(t)}_{\xi,\zeta}$ for $\zeta = 1, 2, \ldots, Z$ based on (31) and (32).
13: Create two new individuals $\mathbf{h}_{\xi,Z+1}$ and $\mathbf{h}_{\xi,Z+2}$ based on (33) and (34), respectively.
14: Evaluate the CE CF of (13) for the two new individuals, obtaining $f_{\xi,Z+1}$ and $f_{\xi,Z+2}$, respectively.
15: **if** $f_{\xi,Z+1} < f_{\xi,Z+2}$ AND $f_{\xi,Z+1} < f_{\text{worst},\xi}$ **then**
16: Replace $\mathbf{h}_{\text{worst},\xi}$ with $\mathbf{h}_{\xi,Z+1}$.
17: **if** $f_{\xi,Z+2} < f_{\text{2nd worst},\xi}$ **then**
18: Replace $\mathbf{h}_{\text{2nd worst},\xi}$ with $\mathbf{h}_{\xi,Z+2}$.
19: **end if**
20: **else if** $f_{\xi,Z+2} < f_{\xi,Z+1}$ AND $f_{\xi,Z+2} < f_{\text{worst},\xi}$ **then**
21: Replace $\mathbf{h}_{\text{worst},\xi}$ with $\mathbf{h}_{\xi,Z+2}$.
22: **if** $f_{\xi,Z+1} < f_{\text{2nd worst},\xi}$ **then**
23: Replace $\mathbf{h}_{\text{2nd worst},\xi}$ with $\mathbf{h}_{\xi,Z+1}$.
24: **end if**
25: **end if**
26: Update $\mathbf{h}_{\text{best},\xi}$, $\mathbf{h}_{\text{worst},\xi}$ and $\mathbf{h}_{\text{2nd worst},\xi}$, along with $f_{\text{best},\xi}$, $f_{\text{worst},\xi}$ and $f_{\text{2nd worst},\xi}$, based on (24), (25) and (26).
27: **end for**
28: $\xi \leftarrow \xi + 1$.
29: **end while**
30: Output $\mathbf{h}_{\text{best},\xi}$ and $f_{\text{best},\xi}$.

The minimum number of CFEs in the DHA is $4.5\sqrt{N}$ and the maximum number of CFEs is $22.5\sqrt{N}$ [27]. In [29], we presented an Early Stopping (ES) modification for the DHA, where we may terminate the DHA before the last $4.5\sqrt{N}$ unnecessary CFEs, where $x_{\min}$, which it will turn out to be equal to x_i, has already been found, but this knowledge is not available to us. In this paper, we will use the ES criterion of [29] in the DHA processes of the proposed QRWBS.

V. QRWBS VERSUS RWBS

The main difference between the RWBS of [17], [19], and [40] and the QRWBS is the methodology adopted for creating the individuals' population Z during each generation ξ with $\xi = 1, 2, \ldots, \Xi$, where the ξth "generation" refers to the number of times the initial individuals' population has been updated. The steps of the RWBS are summarized in Alg. 1, while those of the QRWBS may be found in Alg. 2. The flow

Algorithm 2 Quantum Repeated Weighted Boosting Search for Channel Estimation

Set $\mathbf{h}_{\text{best},0} \leftarrow \mathbf{h}_{p,o-1,\min}, f_{\text{best},0} \leftarrow f_{CE}\left(\mathbf{h}_{p,o-1,\min}, \hat{\mathbf{X}}_o\right)$.
Set $\xi \leftarrow 1$.
while $\xi \leqslant \Xi$ AND $f_{\text{best},\xi-1} - f_{\text{best},\xi} > \Delta_\Xi$ **do**
  Create Z_{DHA} individuals, $\mathbf{h}_{\xi,\zeta}$, $\zeta = 1, 2, \ldots, Z_{DHA}$, based on $\mathbf{h}_{\text{best},\xi-1}$ and according to (23), where Z_{DHA} is a power of 2 and is much higher than the number of individuals in Alg. 1.
  Employ the DHA on the Z_{DHA} individuals and search for $\mathbf{h}_{\text{best},\xi}$, starting from a random $\mathbf{h}_{\xi,\zeta}$ of the Z_{DHA} individuals, based on (13). Stop the DHA after ES number of CFEs.
  The CE CF values of $Z_\xi < ES$ individuals will have been obtained after early stopping the DHA. Include $\mathbf{h}_{\text{best},\xi-1}$ for having a total of $Z_\xi + 1$ individuals.
  $Z \leftarrow Z_\xi + 1$.
  Update $\mathbf{h}_{\text{best},\xi}$ based on (24), along with $f_{\text{best},\xi}$.
  Update $\mathbf{h}_{\text{worst},\xi}$, $\mathbf{h}_{\text{2nd worst},\xi}$ based on (25) and (26), respectively, along with $f_{\text{worst},\xi}$ and $f_{\text{2nd worst},\xi}$.
  Set the weight factors $\delta^{(1)}_{\xi,\zeta}$ to $1/Z$ for all $\zeta = 1, 2, \ldots, Z$.
  for $t_{WBS} = 1, 2, \ldots, T_{WBS}$ **do**
    Normalize the CF values based on (28)
    Calculate the weight factors $\delta^{(t)}_{\xi,\zeta}$ for $\zeta = 1, 2, \ldots, Z$ based on (31) and (32).
    Create two new individuals $\mathbf{h}_{\xi,Z+1}$ and $\mathbf{h}_{\xi,Z+2}$ based on (33) and (34), respectively.
    Evaluate the CE CF of (13) for the two new individuals, obtaining $f_{\xi,Z+1}$ and $f_{\xi,Z+2}$, respectively.
    if $f_{\xi,Z+1} < f_{\xi,Z+2}$ AND $f_{\xi,Z+1} < f_{\text{worst},\xi}$ **then**
      Replace $\mathbf{h}_{\text{worst},\xi}$ with $\mathbf{h}_{\xi,Z+1}$.
      if $f_{\xi,Z+2} < f_{\text{2nd worst},\xi}$ **then**
        Replace $\mathbf{h}_{\text{2nd worst},\xi}$ with $\mathbf{h}_{\xi,Z+2}$.
      end if
    else if $f_{\xi,Z+2} < f_{\xi,Z+1}$ AND $f_{\xi,Z+2} < f_{\text{worst},\xi}$ **then**
      Replace $\mathbf{h}_{\text{worst},\xi}$ with $\mathbf{h}_{\xi,Z+2}$.
      if $f_{\xi,Z+1} < f_{\text{2nd worst},\xi}$ **then**
        Replace $\mathbf{h}_{\text{2nd worst},\xi}$ with $\mathbf{h}_{\xi,Z+1}$.
      end if
    end if
    Update $\mathbf{h}_{\text{best},\xi}$, $\mathbf{h}_{\text{worst},\xi}$ and $\mathbf{h}_{\text{2nd worst},\xi}$, along with $f_{\text{best},\xi}$, $f_{\text{worst},\xi}$ and $f_{\text{2nd worst},\xi}$, based on (24), (25) and (26).
  end for
  $\xi \leftarrow \xi + 1$.
end while
Output $\mathbf{h}_{\text{best},\xi}$ and $f_{\text{best},\xi}$.

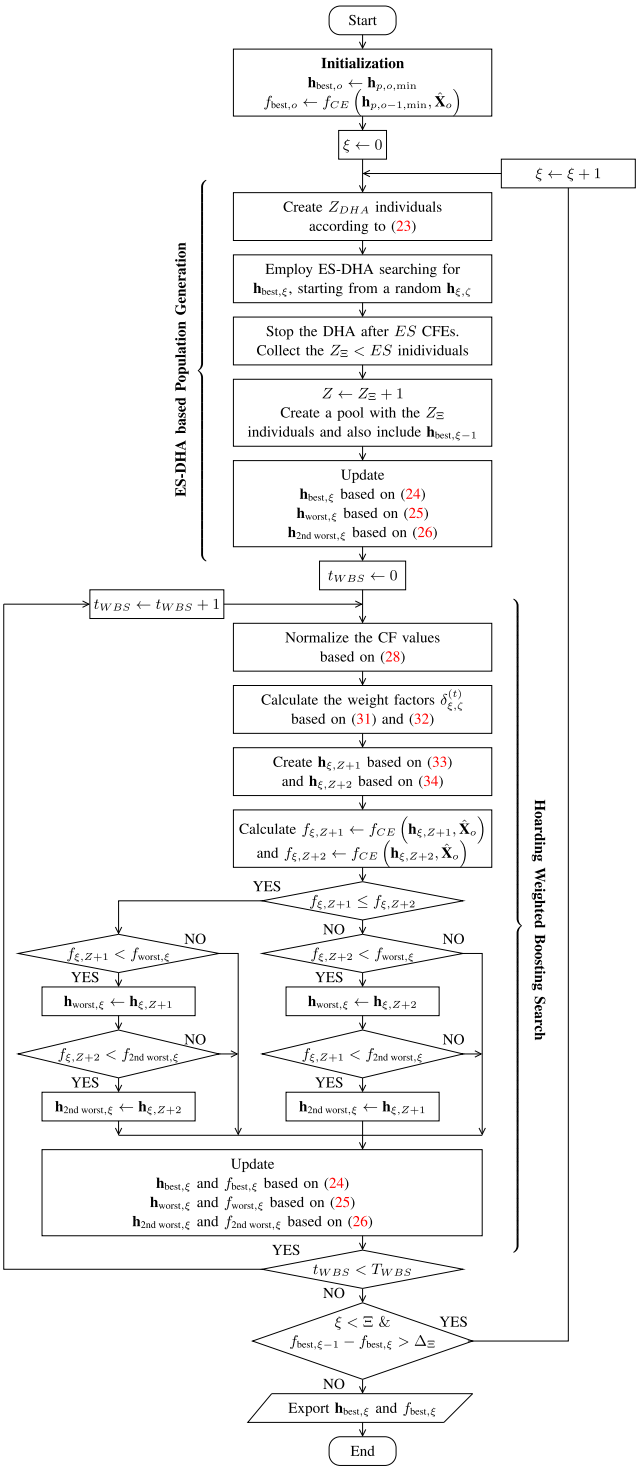

FIGURE 8. Flow chart of the QRWBS.

chart of the QRWBS is presented in Fig. 8. Let us investigate in more depth the stages and differences of the QRWBS and the RWBS, while referring to the channel estimation procedure of the oth OFDM symbol. Both the RWBS and the QRWBS require the number of individuals Z, the number of generations Ξ, the number of weighted boosting searches per generation T_{WBS}, as well as a mutation parameter γ and the required accuracy Δ_Ξ from one generation to the next. The mutation parameter γ scales the effect of the necessary randomness during the update of an individual, while the required accuracy Δ_Ξ determines the threshold difference between the CF value of the best individual of the previous generation and that of the best individual of the present generation, that is accepted, before stopping the search algorithm earlier than Ξ generations. In addition, the RWBS asks for the number of individuals per generation Z, while the QRWBS needs both the number of individuals Z_{DHA}, which will form the search pool of the DHA during each generation

and the maximum allowed number of CF evaluations in the DHA *ES*.

A. STAGE 1 - INITIALIZATION AND POPULATION GENERATION

Initially, both algorithms exploit the predicted CIR of the current oth OFDM symbol $\mathbf{h}_{pr,p,o}$ of (7) and (8), along with its corresponding CE CF value $f_{CE}\left(\mathbf{h}_{pr,p,o}, \hat{\mathbf{X}}_o\right)$, by making them the best so-far found individuals $\mathbf{h}_{\text{best},0}$ and $f_{\text{best},0}$, respectively. From this point on, Stage 1 differs between the RWBS and the QRWBS. The different steps 4, 5 and 6 are marked in blue color in Alg. 1 and Alg. 2.

1) RWBS

During the ξth generation, the best found CIR of the previous $(\xi-1)$th generation is included as one of the Z individuals. The remaining $(Z-1)$ individuals $h_{\xi,\zeta}$ are generated according to

$$\mathbf{h}_{\xi,\zeta} = \mathbf{h}_{\text{best},\xi-1} + \gamma \cdot [\text{randn}\,(UL, 1) + j \cdot \text{randn}\,(UL, 1)], \tag{23}$$

where $\gamma \in \mathbb{R}$ is a mutation parameter and randn(m, n) creates an (m, n)-element matrix with random numbers drawn based on the normal distribution with a zero mean and a unity variance [17]. Having created the population of the ξth generation, the CE CF is evaluated for each of the new $(Z-1)$ individuals according to Step 5 of Alg. 1, resulting in $(Z-1)$ CFEs.

2) QRWBS

However, in the proposed QRWBS we commence by creating Z_{DHA} individuals based on (23) and $\mathbf{h}_{\text{best},\xi-1}$, where Z_{DHA} is a power of 2 and it is higher than the number of individuals in the RWBS. The reason we have opted for creating a much larger pool of individuals is that we perform a quantum search in it using the DHA, for the sake of finding a subset of individuals that are more suitable for our CE search problem. Therefore, Z_{DHA} may assume high values such as 256, 1024 or even 8192 and 32 768. Please note that even though the Z_{DHA} individuals were created by exploiting $\mathbf{h}_{\text{best},\xi-1}$, we have opted for not including this specific CIR vector in the Z_{DHA} individuals, since we have already evaluated its CE CF.

The DHA of Section IV-C is then employed in the set of Z_{DHA} individuals for finding the one that corresponds to the minimum CE CF value of (13), while starting from a random individual. The DHA requires $7.5\sqrt{Z_{DHA}}$ CFEs on average in the quantum domain for finding the wanted individual, when commencing from a random individual [7], [29]. This is why we have included an early stopping criterion [29], where the DHA is terminated after a predetermined number of *ES* CFEs. The individuals and their corresponding CE CF values that will be available to us are the Z_ξ individuals that were evaluated in the classical domain during the DHA. Since *ES* represents the total number of CFEs of a single DHA search, we may expect $Z_\xi < ES < Z_{DHA}$. As the subscript ξ of Z_ξ suggests, we should expect Z_ξ to be different during each generation, since it depends on the probabilistic nature of the DHA and the initial random individual.

Therefore, in the QRWBS we perform *ES* CFEs for obtaining $Z_\xi < ES$ individuals. Even though this may seem disadvantageous, we should note that those Z_ξ individuals are expected to have lower CF values among them than in the case, where they were randomly generated as in the RWBS, since they may be described as a "good" subset of the Z_{DHA} randomly generated individuals. For example, consider the scenario, where $Z-1=99$ individuals were randomly generated based on (23) in RWBS and their CF value was calculated. At the same time, the QRWBS creates $Z_{DHA}=512$ individuals and employs the DHA for them. It should be expected that the probability of having a better individual when the population consists of $Z_{DHA}=5.12\cdot Z$ individuals is higher. By investing $ES=99$ CFEs, the QRWBS has the same complexity as this scenario's RWBS, but it will have obtained on average $Z_\xi=[40, 50]$ individuals, based on our simulations. However, more individuals of the Z_ξ individuals in the QRWBS may exhibit low CF values, when compared to the Z individuals of the RWBS. Moreover, we will discuss that the Weighted Boosting Search (WBS) process is faster when the population Z is smaller and when the selected Z individuals have a lower CF value, which is the case in the QRWBS when compared to the RWBS. The Z_ξ individuals found by the DHA and the best individual of the previous generation $\mathbf{h}_{\text{best},\xi-1}$ will take part in the WBS process of the QRWBS.

From this point onwards, let us omit the subscript ξ from the population of Z_ξ individuals in the QRWBS for simplifying our analysis, and let us denote the number of individuals that take part in the WBS of both the RWBS and the QRWBS as Z, as described in Step 7 of Alg. 2.

In both the RWBS and QRWBS, based on the CF values of the Z individuals, we update $\mathbf{h}_{\text{best},\xi}$, $\mathbf{h}_{\text{worst},\xi}$ and $\mathbf{h}_{\text{2nd worst},\xi}$ along with their respective $f_{\text{best},\xi}$, $f_{\text{worst},\xi}$ and $f_{\text{2nd worst},\xi}$, as in

$$\mathbf{h}_{\text{best},\xi} = \underset{\zeta=1,2,\ldots,Z}{\arg\min}\left\{f_{\xi,\zeta}\right\} \tag{24}$$

$$\mathbf{h}_{\text{worst},\xi} = \underset{\zeta=1,2,\ldots,Z}{\arg\max}\left\{f_{\xi,\zeta}\right\} \tag{25}$$

$$\mathbf{h}_{\text{2nd worst},\xi} = \underset{\zeta=1,2,\ldots,Z\ \&\ \mathbf{h}_{\xi,\zeta}\neq\mathbf{h}_{\text{worst},\xi}}{\arg\max}\left\{f_{\xi,\zeta}\right\}, \tag{26}$$

where

$$f_{\xi,\zeta} = f_{CE}\left(\mathbf{h}_{\xi,\zeta}, \hat{\mathbf{X}}_o\right). \tag{27}$$

B. STAGE 2 - WEIGHTED BOOSTING SEARCH

The WBS process is the same for both the RWBS and the QRWBS. The WBS may be considered as a local optimization search, where new, low-CE CF individuals are generated based on the existing ones in the population. The WBS is repeated T_{WBS} number of times. Before the first iteration, the weight factors, which are used for generating new individuals are initialized as $\delta_{\xi,\zeta}^{(t=0)} = 1/Z$. During the tth iteration, with $t=1, 2, \ldots, T_{WBS}$, the following steps are followed:

1) NORMALIZATION

Initially, the CF values that correspond to the population are normalized according to

$$\bar{f}_{\xi,\zeta} = \frac{f_{\xi,\zeta}}{\sum_{\zeta=1}^{Z} \left(f_{\xi,\zeta}\right)}, \quad \zeta = 1, 2, \ldots, Z. \tag{28}$$

2) UPDATE OF THE WEIGHT FACTORS

Using the normalized CF values of (28) and the weight factors of the previous WBS iteration $\delta_{\xi,\zeta}^{(t-1)}$, we compute

$$\eta_{\xi}^{(t)} = \sum_{\zeta=1}^{Z} \left(\delta_{\xi,\zeta}^{(t-1)} \cdot \bar{f}_{\xi,\zeta}\right), \tag{29}$$

$$\beta_{\xi}^{(t)} = \frac{\eta_{\xi}^{(t)}}{1 - \eta_{\xi}^{(t)}}. \tag{30}$$

The weight factors $\delta_{\xi,\zeta}^{(t)}$ are updated according to [17], [19]

$$\delta_{\xi,\zeta}^{(t)} = \begin{cases} \delta_{\xi,\zeta}^{(t-1)} \cdot \left(\beta_{\xi}^{(t)}\right)^{\bar{f}_{\xi,\zeta}} & \beta_{\xi}^{(t)} \leqslant 1 \\ \delta_{\xi,\zeta}^{(t-1)} \cdot \left(\beta_{\xi}^{(t)}\right)^{1-\bar{f}_{\xi,\zeta}} & \beta_{\xi}^{(t)} > 1. \end{cases} \tag{31}$$

Finally, the updated weight factors are normalized as in

$$\delta_{\xi,\zeta}^{(t)} = \frac{\delta_{\xi,\zeta}^{(t)}}{\sum_{\zeta=1}^{Z} \delta_{\xi,\zeta}^{(t)}}. \tag{32}$$

Let us provide some intuition about the variables $\eta_{\xi}^{(t)}$, $\beta_{\xi}^{(t)}$ and $\delta_{\xi,\zeta}^{(t)}$. The variable $\eta_{\xi}^{(t)}$ provides a weighted sum of the normalized CF values of the population. Since initially each individual has the same weight $\delta_{\xi,\zeta}^{(0)} = 1/Z$ for $\zeta = 1, 2, \ldots, Z$ and $\sum_{\zeta=1}^{Z} \left(\bar{f}_{\xi,\zeta}\right) = 1$ is always true, we have $\eta_{\xi}^{(1)} = 1/Z$ and hence $\beta_{\xi}^{(1)} = 1/(Z-1)$ for every generation $\xi = 1, 2, \ldots, \Xi$. Therefore, the higher Z, the lower the initial values of $\eta_{\xi}^{(1)}$ and $\beta_{\xi}^{(1)}$. Commencing from these values of $\eta_{\xi}^{(1)}$ and $\beta_{\xi}^{(1)}$, both the QRWBS and the RWBS are started by updating the weight factors $\delta_{\xi,\zeta}^{(t)}$. Since the normalized CF values are also used for updating the weight factors $\delta_{\xi,\zeta}^{(t)}$, we may expect that the higher Z is, the smaller the differences between $\bar{f}_{\xi,\zeta}$, $\zeta = 1, 2, \ldots, Z$ become, indicating a slower dissociation of $\delta_{\xi}^{(t)} = \left[\delta_{\xi,1}^{(t)}, \ldots, \delta_{\xi,Z}^{(t)}\right]^T$ with respect to the uniform distribution of $\delta_{\xi}^{(0)}$.

It should be noted that a "better" individual is associated with a lower CF value and hence a higher weight factor according to (31) and (32). Hence, as the WBS iteration index t increases, $\eta_{\xi}^{(t)}$ depends more on the "better" individuals, which have a lower CF value and a higher weight factor by then.

3) CONVEX COMBINATION

Having updated the weight factors $\delta_{\xi,\zeta}^{(t)}$ during the tth WBS iteration, we create two new individuals, namely $\mathbf{h}_{\xi,Z+1}$ and $\mathbf{h}_{\xi,Z+2}$, based on a convex combination of the Z existing individuals, as in

$$\mathbf{h}_{\xi,Z+1} = \sum_{\zeta=1}^{Z} \delta_{\xi,\zeta}^{(t)} \cdot \mathbf{h}_{\xi,\zeta} \tag{33}$$

$$\mathbf{h}_{\xi,Z+2} = \mathbf{h}_{\text{best},\xi} + \left(\mathbf{h}_{\text{best},\xi} - \mathbf{h}_{\xi,Z+1}\right), \tag{34}$$

where (34) may be considered as the mirrored individual with respect to the "best so far found" individual $\mathbf{h}_{\text{best},\xi}$. Referring to (33), we may observe that the specific individuals, which are associated with a higher weight factor are more involved in the creation of the $(Z+1)$th individual.

4) UPDATING THE POPULATION

The new pair of individuals may replace existing individuals in the population. In the literature [17], [19], [40], the specific new individual, which is associated with a higher CF value, replaces the worst individual in the population, regardless of the CF value of the latter. Both the previously worst individual in the population and the worse individual of the new pair are then discarded.

In this paper we propose a different approach for updating the population during each WBS iteration. Firstly, we replace the worst individual in the population with the better individual of the new pair of individuals, only if this new individual is also better than the worst individual in the existing population. Moreover, if this replacement was successful, we proceed by replacing the second worst individual in the existing population with the worse individual of the new pair of individuals, only if that worse individual of the new pair of individuals is associated with a lower CF value than that of the second worst individual in the population. This methodology is summarized in Steps $16-26$ of Alg. 2 and in the flow chart of Fig. 8. By potentially exploiting both new individuals we expect to exhibit a faster convergence of the WBS, or equivalently, anticipate arriving at a better individual $\mathbf{h}_{\text{best},\xi}$ after a predetermined number T_{WBS} of WBS iterations.

Finally, before starting the next $(t+1)$th WBS iteration, we update the best, worst and second worst individuals of the population according to (24), (25) and (26).

C. STAGE 3 - TERMINATION

After T_{WBS} iterations of the WBS in the ξth generation, the "best so-far found" individual $\mathbf{h}_{\text{best},\xi}$ is saved and the WBS loop is terminated. Based on the predetermined maximum number of generations Ξ and also on the predetermined CF accuracy Δ_{Ξ} between generations, we employ a pair of termination criteria:

1) If $\xi = \Xi$, we have created and investigated the maximum number of allowed generations.
2) If the best CE CF value of the current ξth generation is close to the best CE CF value of the previous $(\xi-1)$th

generation, as encapsulated in $f_{\text{best},\xi-1} - f_{\text{best},\xi} \leqslant \Delta_\Xi$, the required accuracy has been reached.

If neither of the above criteria is activated, we increment the value of ξ by one and start the next generation of the RWBS or QRWBS as stated in Section V-A1 or Section V-A2, respectively. If either of the above criteria is fulfilled, then the RWBS or the QRWBS outputs $\mathbf{h}_{p,o,\min} = \mathbf{h}_{\text{best},\xi}$ as the best found CIR and terminates.

VI. COMPLEXITY OF THE QRWBS AND RWBS

Initially, both the RWBS and the QRWBS perform a single CFE for determining the CF value of the initial CE and the output of the MUD. During every generation, the RWBS performs $(Z-1)$ CFEs for creating the new population of individuals, and $2 \cdot T_{WBS}$ additional CFEs, since a pair of new individuals is created during each of the T_{WBS} iterations. Therefore, the number of CFEs per OFDM symbol of the RWBS after the Ξth generation is [17], [19]

$$\mathcal{C}_{RWBS} = [1 + \Xi \cdot (Z - 1 + 2 \cdot T_{WBS})] \cdot P. \quad (35)$$

Therefore, the complexity of the RWBS depends on the number of generations Ξ, on the number of individuals Z and on the number of WBS iterations T_{WBS}.

Similarly, the DHA in every generation of the QRWBS is stopped after a predetermined number of ES CFEs. Furthermore, the QRWBS also requires $2 \cdot T_{WBS}$ CFEs in the WBS stage, as the RWBS. In total, the number of CFEs per OFDM symbol of the QRWBS after the Ξth generation is

$$\mathcal{C}_{QRWBS} = [1 + \Xi \cdot (ES + 2 \cdot T_{WBS})] \cdot P. \quad (36)$$

By comparing (35) to (36), we may observe that if we set $ES = Z - 1$, the QRWBS imposes the same complexity as the RWBS.

It should be mentioned that unless stated otherwise, we allow multiple MUD-CE iterations only during the first MUD-CE-DEC iteration. Therefore, in a system the MUD and the CE are activated I_{CE}^{MUD} times only during the first $I_{DEC}^{MUD-CE} = 1$ MUD-CE-DEC iteration and only once during the subsequent MUD-CE-DEC iterations. The reason for following this methodology is that of reducing the complexity of the system, since it will be demonstrated in Fig. 21, that after the decoders have started operating, performing more than one MUD-CE iterations during a subsequent MUD-CE-DEC iteration may not be sufficiently beneficial for justifying the additional complexity. Moreover, during the last MUD-CE-DEC iteration, there is no need for performing the CE again, because its CIR estimates will not be exploited, since they would only be used by the MUD of a potentially subsequent MUD-CE-DEC iteration. Therefore, unless stated otherwise, in a system with I_{CE}^{MUD} MUD-CE iterations and I_{DEC}^{MUD-CE} MUD-CE-DEC iterations, in total the MUD is employed $(I_{CE}^{MUD} + I_{DEC}^{MUD-CE} - 1)$ times, the CE is invoked $(I_{CE}^{MUD} + I_{DEC}^{MUD-CE} - 2)$ times and the decoders I_{DEC}^{MUD-CE} times.

TABLE 2. Parameters of the multi-user SDMA-OFDM systems.

Number of Users	$U = 4, 6, 8$
Number of AEs per User	$N_{T_x} = 1$
Number of AEs at the BS	$P = 2, 4$
Modulation	QPSK $M = 4$
Channel Code	Turbo Convolutional Code, $R = 1/2$, 8 Trellis states $I_{inner} = 4$ inner iterations
Spreading Factor	$SF = 1$
Number of Subcarriers	$Q = 1024$
Cyclic Prefix	CP = 128
Number of Subcarriers per User	$W = 1024$
Normalized User Load	$U_L = U \cdot N_{T_x} \cdot W/(P \cdot Q) = 2, 3, 4$
Interleaver Length	$\{8\,192, 17\,408\}$ per User
Pilot OFDM Symbol every	Δ_t=$\{8, 17\}$ OFDM symbols
Channel Model	EVA, ETU [41]
Mobile Velocity	$v = 30, 130$ km/h
Sampling Frequency	$f_s = 15.36$ MHz
Carrier Frequency	$f_c = 2.5$ GHz
Normalized Doppler Frequency	$f_d = 5.27 \cdot 10^{-6}, 1.96 \cdot 10^{-5}$
Effective Normalized Doppler Frequency	$F_d = Q \cdot f_d \in 0.005, 0.02$
Pilot Channel Estimation Sequence	Optimal [1], [4]
Number of Prediction Filter's Taps	$N_{tap} = 0, 1, 2, 4, 8$
Pilot OFDM symbol's E_b/N_0	same as Data OFDM symbol's

TABLE 3. Parameters of the RWBS and QRWBS.

	RWBS	QRWBS
Number of Individuals	$Z = 100$	$Z_{DHA} = 512$
Number of CFEs before Early Stopping	N/A	$ES = 99$
Number of Generations Ξ	300	300
Mutation Parameter γ	0.01	0.01
Number of WBS Iterations T_{WBS}	20	20
Generation Accuracy Δ_Ξ	0, 10^{-4}	0, 10^{-4}

VII. SIMULATION RESULTS

The parameters of the systems that will be investigated are summarized in Table 2. The default parameters of the RWBS and the QRWBS employed in our systems are summarized in Table 3. Let us commence in Section VII-A by investigating the MSE performance of (13), when no iterations are allowed between the MUD, the CE and the decoders, corresponding to $I_{CE}^{MUD} = 1$ and $I_{DEC}^{MUD-CE} = 1$. Let us compare the performance of the QRWBS to that of the RWBS, while characterizing the impact of the proposed generation update methodology, of the normalized effective Doppler frequency F_d, of the power delay profile of the channels, of the number of users, of the signal to noise ratio, of the prediction filter's length and finally of the initial population of the QRWBS have on the resultant MSE. In Section VII-B we will discuss the BER performance of the selected multi-user systems for

comparing the QRWBS to the RWBS based on the aforementioned parameters.

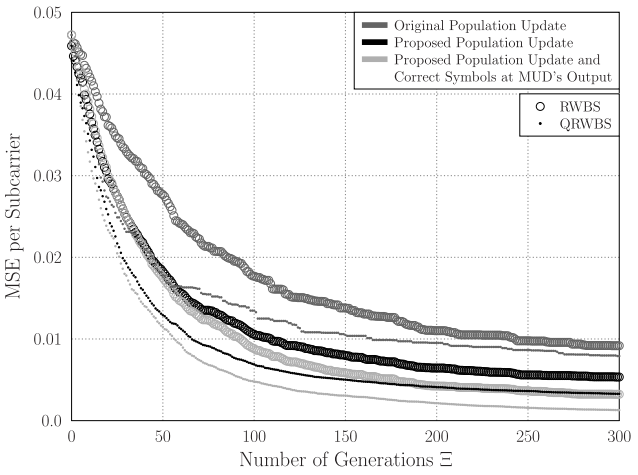

FIGURE 9. Average MSE performance of the first data OFDM symbol, following the pilot OFDM symbol in a noiseless scenario, when the RWBS-aided and the QRWBS-aided CE have been employed with the original population update [17], [19], [40], as well as the proposed population update. The system supports $U = 4$ users transmitting over the ETU channel with $F_d = 0.02$ and an $N_{tap} = 1$ tap CIR predictor was used. There were 60 symbol errors at the output of the MAP MUD, due to the high normalized effective Doppler frequency F_d. The MSE corresponds to the CE of the channels of the $P = 2$ receive AEs. The MSE performance in the hypothetical scenario, where the symbols at the output of the MAP MUD were correct is also included as a best case scenario reference.

A. MSE PERFORMANCE

In Fig. 9 we depict the MSE performance of (13) for the channels that correspond to the $P = 2$ receive AEs, when the proposed population update or the original population update [17], [19], [40] are used, in noiseless scenarios where $U = 4$ users are supported who transmit over ETU channels having a normalized effective Doppler frequency of $F_d = 0.02$. A single-tap CIR prediction filter is selected for providing an initial estimate of the CIR in the data symbol. At the output of the MAP MUD, which operated with the aid of the predicted CIR, which in turn was based on the estimated channels of the previous pilot OFDM symbol, there were 60 symbol errors, due to the high effective normalized Doppler frequency F_d. The idealized unrealistic scenario where error-free symbol references are available at the output of the MAP MUD is also illustrated in Fig. 9. We may observe that the QRWBS-aided CE performs better than the RWBS-aided CE in all three scenarios in terms of converging to a CIR with a lower MSE. Furthermore, both the RWBS-aided CE and the QRWBS-aided CE relying on the proposed population update outperform their counterparts, which use the original population update. Moreover, in the early generations, the QRWBS-aided CE associated with the original population update succeeds in finding a CIR with lower MSE than that found by the RWBS-aided CE in conjunction with the proposed population update. As it was expected, when error-free symbol references are available at the input of the CE, the estimated CIRs exhibit a lower MSE. Note that if we do not apply iterations between the MUD and the CE, the 60 erroneous symbols will not be corrected at this stage, they will be forwarded to the decoder, and the channel estimate of the OFDM symbol will be calculated based on an erroneous symbol vector X, which may result in avalanche-like error propagation during the subsequent OFDM symbols.

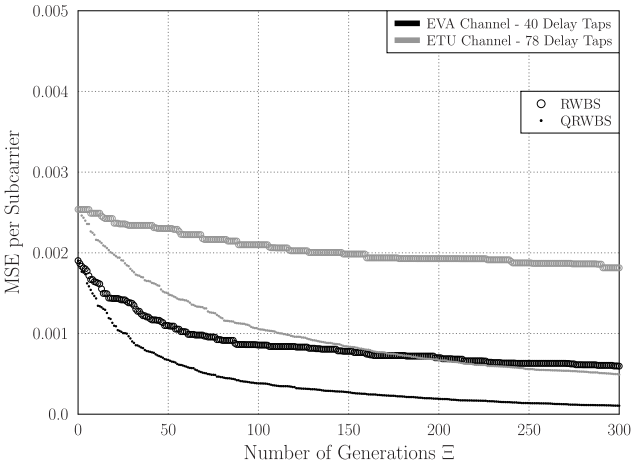

FIGURE 10. Average MSE performance of the first data OFDM symbol, following the pilot OFDM symbol in a noiseless scenario, when the RWBS-aided and the QRWBS-aided CE have been employed in EVA and ETU channels, both experiencing the same effective normalized Doppler frequency of $F_d = 0.0046$, which corresponds to a user velocity of $v = 30$ km/h. The system supports $U = 4$ users and the MSE corresponds to the CE of the channels of the $P = 2$ available receive AEs at the BS. An $N_{tap} = 1$ tap CIR predictor was used. There were 0 errors at the output of the MAP MUD in both scenarios. The last path in the EVA channel arrives at the $L = 40$th delay tap, while that of the ETU channel arrives at the $L = 78$th delay tap.

Following the same system setup as in Fig. 9 with the only difference that the vehicular speed is now $v = 30$ km/h, corresponding to $F_d = 0.0046$, Fig. 10 shows the MSE of (13) when two channels associated with different power delay profile are used, namely the Extended Vehicular A (EVA) and the Extended Typical Urban (ETU) channels [41]. The last paths in the EVA and ETU channels arrive at the $L_{EVA} = 40$th and $L_{ETU} = 78$th delay tap, respectively. Again, the MSE in Fig. 10 was calculated for noiseless scenarios supporting $U = 4$ users and it corresponds to the CIR estimated for the $P = 2$ receive AEs at the BS, while a single tap ($N_{tap} = 1$) CIR predictor was employed for the *a priori* estimation of the CIR based on the data OFDM symbol. It should be noted that in contrast to Fig. 9, the MAP MUD in Fig. 10 offered an error-free symbol sequence at its output, since the normalized effective Doppler frequency F_d is sufficiently low in these scenarios. The QRWBS-aided CE performs better than the RWBS-aided CE and the gain is higher, when we have more unknown variables, as in the case of the ETU channel, where $U \cdot L_{ETU} = 312$ unknown CIR variables have to be estimated, in contrast to the $U \cdot L_{EVA} = 160$ unknown variables of the EVA channel.

The MSE performance illustrated in Fig. 11 was simulated based on the same noiseless scenarios, with the difference

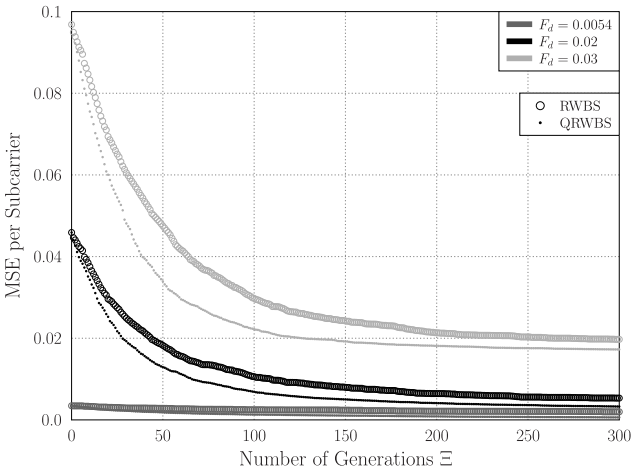

FIGURE 11. Average MSE performance of the first data OFDM symbol, following the pilot OFDM symbol in a noiseless scenario, when the RWBS-aided and the QRWBS-aided CE have been employed in ETU channels, when the effective normalized Doppler frequency varies between $F_d = 0.0054, 0.02, 0.03$. The system supports $U = 4$ users and the MSE corresponds to the CE of the channels of the $P = 2$ available receive AEs at the BS. An $N_{tap} = 1$ tap CIR predictor was used. There were 0, 60 and 268 symbol errors on average at the output of the MAP MUD, when $F_d = 0.0054$, 0.02 and 0.03, respectively.

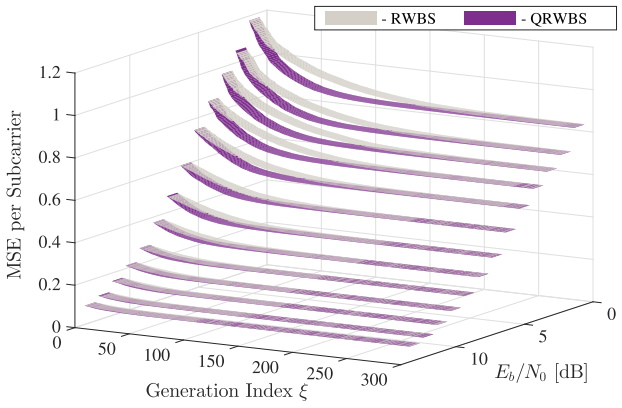

FIGURE 12. Average MSE performance of the first data OFDM symbol, following the pilot OFDM symbol, when the RWBS-aided and the QRWBS-aided CE have been employed in EVA channels with $F_d = 0.005$ for various E_b/N_0 values. The system supports $U = 4$ users and the MSE corresponds to the CE of the channels of the $P = 2$ receive AEs. An $N_{tap} = 1$ tap CIR predictor was used. There were 1836, 1730, 1616, 1529, 1381, 1245, 1103, 919, 724, 582, 421, 339 and 236 symbol errors on average at the output of the MAP MUD, when $E_b/N_0 = 0, 1, \ldots, 12$, respectively.

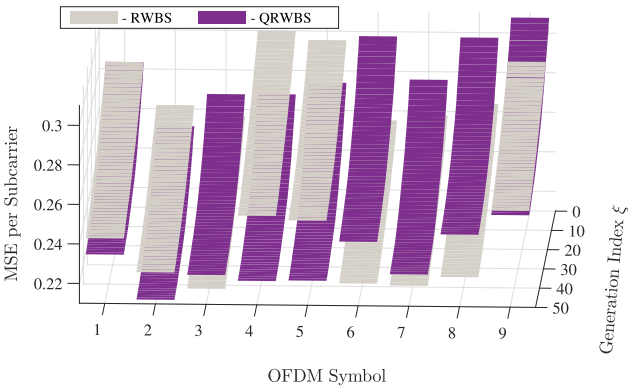

FIGURE 13. Instantaneous MSE performance of the first 9 data OFDM symbols, with the first one following the pilot OFDM symbol, when the RWBS-aided and the QRWBS-aided CE have been employed in EVA channels with $F_d = 0.005$ for $E_b/N_0 = 8$ dB and $\Xi = 50$ generations per search. The system supports $U = 4$ users and the MSE corresponds to the CE of the channels of the first receive AE among the $P = 2$ available receive AEs at the BS. No CIR predictor was used in this system.

that only the ETU channel is employed and the normalized effective Doppler frequency F_d varies between $F_d = 0.0054, 0.02, 0.03$. It is reasonable for the MSE to increase when F_d increases, even in noiseless scenarios, since the initial channel estimate, which was used in the MAP MUD was predicted based on the previous OFDM symbol and the higher the system's F_d, the more different the CIRs of two consecutive OFDM symbols are. This phenomenon makes the CIR prediction more difficult and it may lead to error propagation. In the particular example of Fig. 11, there were 0, 60 and 268 erroneously detected symbols on average at the output of the MAP MUD when $F_d = 0.0054, 0.02, 0.03$, respectively. Nevertheless, regardless of the value of F_d, the QRWBS-aided CE succeeds in finding a CIR associated with a lower MSE, when compared to the RWBS-aided CE.

In Fig. 12 the MSE performance of a similar system is presented, where EVA channels associated with $F_d = 0.005$ are used and E_b/N_0 varies from 0 dB to 12 dB. The MSE corresponds to the first data OFDM symbol and to the $P = 2$ receive AEs, when $U = 4$ users are supported by the system. The MSE becomes lower as E_b/N_0 increases. The QRWBS always performs better than the RWBS, by converging faster to a usually better CIR. When E_b/N_0 increases, the MSE gain of both the QRWBS and the RWBS is decreased, but the number of CFEs required by the QRWBS for convergence is still lower than that of the RWBS. Please note that the estimated CIRs correspond to the erroneous symbol vectors detected by the MAP MUD, which may lead to error propagation, as reserved in Fig. 13.

In Fig. 13, we present the instantaneous MSE performance of the RWBS-aided and QRWBS-aided CEs in the same system as that investigated in Fig. 12, when operating at $E_b/N_0 = 8$ dB for the first 9 data OFDM symbols, without using a CIR prediction filter. At the first data OFDM symbol, the QRWBS converges faster than the RWBS and to a CIR associated with lower MSE. It should be noted that both the RWBS and the QRWBS estimated a CIR for the first OFDM symbol based on an erroneous detected symbol vector at the output of the MAP MUD. During the second data OFDM symbol, both the detected symbol vectors of the two systems include symbol errors and they are different from each other. This may lead to error propagation and it may not be capable of exploiting the fast convergence speed of the QRWBS to a better CIR, as it may be seen in the third data OFDM symbol, where the QRWBS starts from and also converges to a CIR with a higher MSE value than that of the RWBS. Recall that the RWBS and the QRWBS performed CE based

on a different symbol vector $\mathbf{X}$. Therefore, the power of the QRWBS is demonstrated to be better in scenarios, where the detected symbol vector contains a few symbol errors, for avoiding error propagation. An interesting example is constituted by the 9th data OFDM symbol, where the MSE of the initial CIR in the QRWBS system has a higher MSE value than the respective one of the RWBS system, again while using a different detected symbol vector. Eventually, the QRWBS finds a CIR with a lower MSE than the CIR that the RWBS converges to. Using a CIR prediction filter would have improved the initial CIR estimate of a data OFDM symbol, which in turn might have resulted in a better symbol vector detected by the MAP MUD and hence a better CE performance.

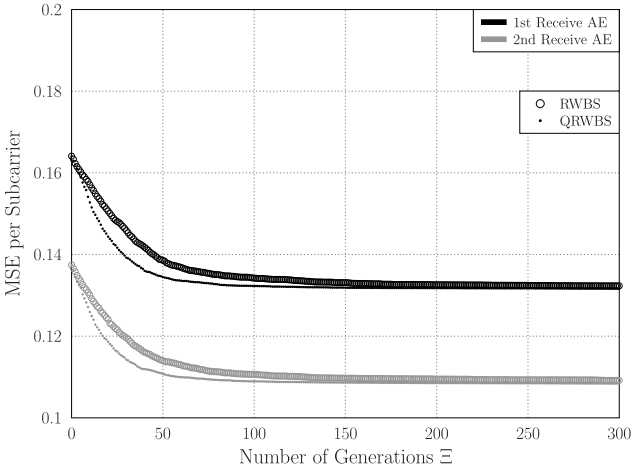

FIGURE 14. Instantaneous MSE performance of the first data OFDM symbol, following the pilot OFDM symbol, when the RWBS-aided and the QRWBS-aided CE have been employed in EVA channels with $F_d = 0.005$, while $E_b/N_0 = 10$ dB for both receive AEs. The system supports $U = 4$ users and an $N_{tap} = 1$ tap CIR predictor was employed.

Fig. 14 compares the instantaneous MSE performance of the CE concerning the first data OFDM symbol for the channels related to the first and second receive AE, when the RWBS and QRWBS are employed, while $E_b/N_0 = 10$ dB and a single-tap CIR predictor is used. Since the instantaneous AWGN at each receive AE is different, the initial MSE is also expected to differ. However, the trend of the MSE with respect to the number of generations Ξ in the RWBS and the QRWBS is similar, indicating that the QRWBS converges faster than the RWBS, regardless of the channels that are estimated.

If we vary the number of individuals that take part in the DHA Z_{DHA} in the QRWBS, while using the same early stopping criterion in terms of the number of affordable CFEs ES in each generation's DHA, we may expect to obtain a better CIR when the Z_{DHA} is increased, since a larger population will have been searched. At the same time, the complexity of the QRWBS should remain the same, since, according to (36), it does not depend on Z_{DHA}, but rather on ES. By observing Fig. 15, we may conclude that the gain is higher when the pool

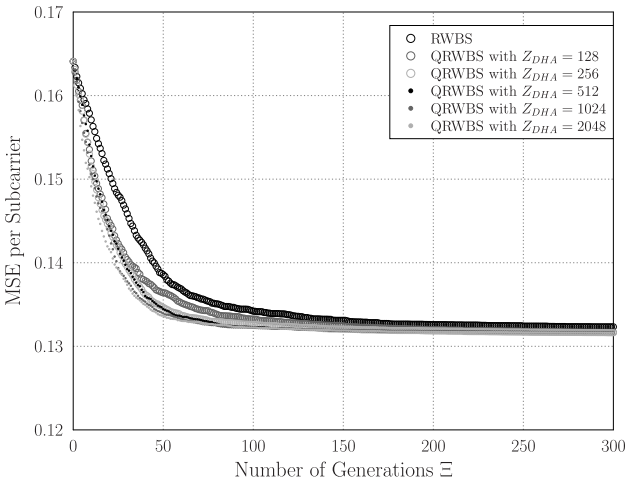

FIGURE 15. Average MSE performance of the first data OFDM symbol, following the pilot OFDM symbol, when the RWBS-aided and the QRWBS-aided CE have been employed in EVA channels with $F_d = 0.005$ for $E_b/N_0 = 10$ dB for the channels of the $P = 2$ receive AEs, when the number of individuals in the QRWBS varies between $Z_{DHA} = 128, 256, 512, 1024, 2048$. The system supports $U = 4$ users and the DHA in each generation of the QRWBS is stopped after $ES = 99$ CFEs. Therefore, the complexity of each of the depicted QRWBS, as well as that of the RWBS is the same and equal to 139 CFEs per generation. An $N_{tap} = 1$ tap CIR predictor was employed.

of searched individuals Z_{DHA} increases. The exact gain value is expected to vary depending on the selected value of ES. Let us choose $Z_{DHA} = 512$ for our next simulations.

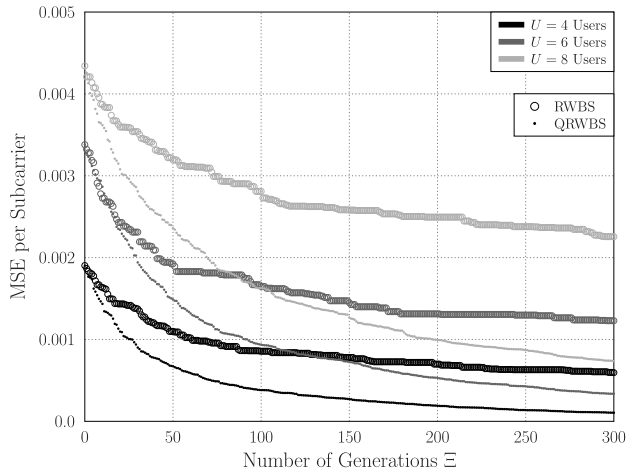

FIGURE 16. Average MSE performance of the first data OFDM symbol, following the pilot OFDM symbol in a noiseless scenario, when the RWBS-aided and the QRWBS-aided CE have been employed in EVA channels with $F_d = 0.005$. The systems support $U = 4, 6$ or 8 users and the MSE corresponds to the CE of the channels of the $P = 2$ receive AEs. An $N_{tap} = 1$ tap CIR predictor was employed. The pilot and data OFDM symbols transmitted by the first 4 users in all systems are the same. Similarly, the pilot and data OFDM symbols of the fifth and sixth users in the systems, where $U = 6$ and $U = 8$ users are supported, are also the same. The number of symbol errors at the output of the MAP MUD is 0, 9 and 93 on average for the systems where $U = 4, 6$ and 8 users were supported, respectively.

Fig. 16 presents the MSE performance of the RWBS-aided and QRWBS-aided CE for the first data OFDM symbol, when

$U = 4$, 6 and 8 users are supported by the noiseless systems, where EVA channels with $F_d = 0.005$ are used. The MSE corresponds to the $P = 2$ receive AEs and a $N_{tap} = 1$ tap CIR predictor was used. In all systems the QRWBS performs better than the RWBS, since it converges to a CIR with a lower MSE value. As expected, the MSE gain of the system, where $U = 8$ users are supported is higher, since $U \cdot L = 320$ unknown variables have to be estimated, compared to the 240 and 160 CIR variables that have to be estimated when $U = 6$ and $U = 4$ users are supported, respectively. In fact, even though the estimated CIRs of the systems, where $U = 6$ and $U = 8$ users are supported, are found based on an erroneous symbol vector at the output of the MAP MUD, their MSE is very close to that of the CIR estimated by the RWBS in the system, where $U = 4$ users are supported.

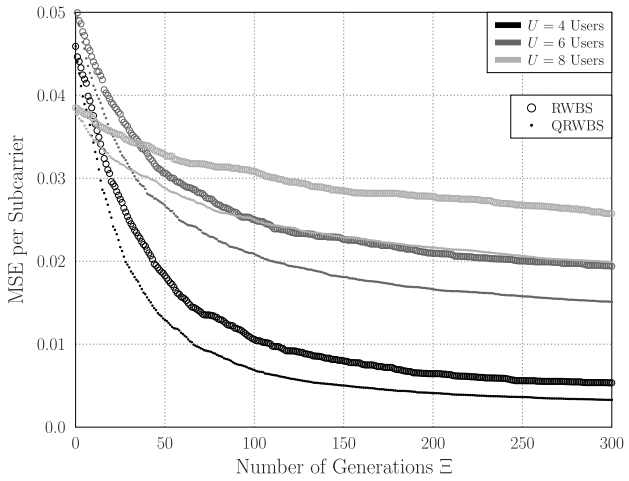

FIGURE 17. Average MSE performance of the first data OFDM symbol, following the pilot OFDM symbol in a noiseless scenario, when the RWBS-aided and the QRWBS-aided CE have been employed in ETU channels. The systems support $U = 4$, 6 or 8 users and the MSE corresponds to the CE of the channels of the $P = 2$ receive AEs. An $N_{tap} = 1$ tap CIR predictor was employed. The pilot and data OFDM symbols transmitted by the first 4 users in all systems are the same. Similarly, the pilot and data OFDM symbols of the fifth and sixth users in the systems, where $U = 6$ and $U = 8$ users are supported, are also the same. The number of symbol errors at the output of the MAP MUD is 60, 784 and 3208 on average for the systems where $U = 4$, 6 and 8 users are supported, respectively.

In Fig. 17 we characterize the same systems as in Fig. 16, with the difference that the users transmit over ETU channels associated with $F_d = 0.02$. As in Fig. 16, in all the systems characterized in Fig. 17 the QRWBS performs better than the RWBS, since it converges to a CIR with a lower MSE value. The initial MSE of the systems, where $U = 4$ and $U = 6$ users are supported is higher in the ETU channel than in the EVA channels of Fig. 16, since the normalized effective Doppler frequency is higher in these scenarios and the CE was based on a detected symbol vector with more symbol errors. On the other hand, the initial MSE value of the system, where $U = 8$ users are supported is slightly lower than that of Fig. 16, due to the fact that the number of symbol errors was already high in the EVA channels. Comparing the MSE behaviour of the QRWBS and the RWBS in the ETU channels of Fig. 17 and EVA channels of Fig. 16, both algorithms converge more slowly, since 312, 468 and 634 continuous random variables have to be estimated when $U = 4$, 6 and 8 users, respectively, transmit over ETU channels. Therefore, for a fixed number of users, the number of CIR variables that have to be estimated when ETU channels are used is almost twice as high as the number of continuous CIR variables that have to be found when EVA channels are used. Furthermore, in the systems communicating over the ETU channels, the convergence results in a higher MSE value, since the symbol vector at the output of the MAP MUD contains more symbol errors. The number of symbol errors becomes even higher when more users are supported.

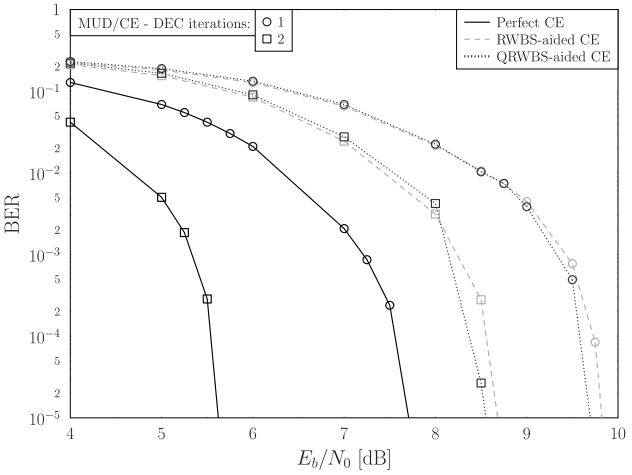

FIGURE 18. BER performance of an SDMA-OFDM system supporting $U = 4$ users with $P = 2$ receive AEs, transmitting over EVA channels, when perfect CE is available, as well as when the RWBS and the QRWBS are employed for CE. The CIR prediction filter's order is equal to $N_{tap} = 4$, $I_{CE}^{MUD} = 2$ iterations are allowed between the MAP MUD and the CE and $I_{DEC}^{MUD-CE} = 2$ iterations are allowed between the MUD-CE and the decoders. The interleaver length is 17 408 bits and a pilot OFDM symbol is transmitted every 17 data OFDM symbols. The rest of the parameters are stated in Table 2 and Table 3.

B. BER PERFORMANCE

In Fig. 18 we compare the performance of the RWBS-aided and QRWBS-aided CEs in a rank-deficient system, where $U = 4$ users are supported and $P = 2$ receive AEs are available at the BS, when transmitting over EVA channels. We have opted for a CIR prediction filter of $N_{tap} = 4$th order and $I_{CE}^{MUD} = 2$ iterations are allowed between the MAP MUD and the CE, while $I_{DEC}^{MUD-CE} = 2$ iterations are performed between the MUD-CE and the decoders, as illustrated in Fig. 2. The generation accuracy Δ_Ξ has been set to 10^{-4} and the maximum number of generations is $\Xi = 300$. The rest of the parameters are summarized in Table 2 and Table 3. The CIR prediction filter provides a sufficiently accurate initial estimate for the EVA channels, which are associated with a relatively low normalized Doppler frequency F_d.

The QRWBS-aided CE performs better than the RWBS-aided CE, especially in the low-BER region, where

there is a 0.2 dB gain for the QRWBS-aided CE. Even though this performance improvement is not substantial, it is worth noticing that it is associated with a lower complexity for the QRWBS-aided CE, when compared to that of the RWBS-aided CE. In more detail, according to Section VI, after one MUD-CE-DEC iteration, the CE has been employed $I_{CE}^{MUD} = 2$ times for each of the $P = 2$ receive AEs, resulting in a total of 16 667 CFEs per data OFDM symbol for the QRWBS-aided CE and 20 114 CFEs per data OFDM symbol for the RWBS-aided CE, when operating at an E_b/N_0 value that corresponds to a BER of 10^{-5}. Therefore, the QRWBS-aided CE achieves a slightly better BER performance than the RWBS-aided CE in the system of Fig. 18, at 83% of the complexity imposed by the RWBS-aided CE.

When compared to the performance of the system, assuming that perfect CIR estimates are available, there is a ∼0.8 dB E_b/N_0 loss between the system using the QRWBS-aided CE and the system associated with perfect CE and $J = 1$ iteration between the MUD and the decoders, where J is the number of MUD-DEC iterations when perfect CE is available. The associated performance discrepancy becomes 3 dB when 2 MUD-DEC iterations are allowed in the system having perfect CE. This was expected, since when imperfect CE is available and DDCE is employed, error propagation will occur, hence resulting in a degraded performance compared to that of the system having perfect CE.

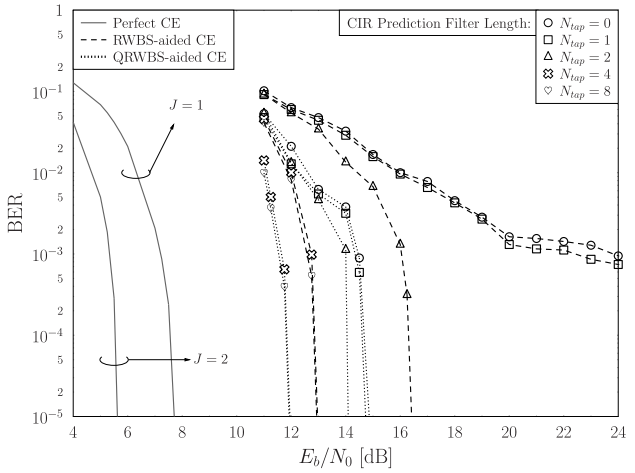

FIGURE 19. BER performance of an SDMA-OFDM system supporting $U = 4$ users with $P = 2$ receive AEs, transmitting over ETU channels, when perfect CE is available, as well as when the RWBS and the QRWBS are employed for CE. The CIR prediction filter's order varies between $N_{tap} = 0, 1, 2, 4, 8$, $I_{CE}^{MUD} = 3$ iterations are allowed between the MAP MUD and the CE and $I_{DEC}^{MUD-CE} = 2$ iterations are allowed between the MUD-CE and the decoders. The interleaver length is 8 192 bits and a pilot OFDM symbol is transmitted every 8 data OFDM symbols. The rest of the parameters are stated in Table 2 and Table 3.

In Fig. 19, the same system is employed, with the differences that now ETU channels are used, associated with $F_d = 0.02$, the interleaver length is 8 192 bits, $I_{DEC}^{MUD-CE} = 2$ and the number of iterations between the MAP MUD and the CE during the first MUD-CE-DEC iteration is $I_{CE}^{MUD} = 3$. We may observe that the QRWBS-aided CE always performs better than the RWBS-aided CE. More precisely, in the scenarios, where either no CIR prediction filter or a first-order CIR prediction filter is employed, the QRWBS-aided CE systems reach a BER of 10^{-5} at $E_b/N_0 = 15$ dB, while the RWBS-aided CE systems experience an error floor at a BER of 10^{-3}. This shows that the QRWBS-aided CE is more resilient to a high normalized effective Doppler frequency F_d than the RWBS-aided CE. When the order N_{tap} of the CIR prediction filter is increased, the performance is improved, with the RWBS-aided CE systems benefiting more. In other words, the QRWBS-aided system performs better than the RWBS-aided system by a margin of 2.2 dB when a second order CIR prediction filter is used, while there is a 1 dB performance gain for the QRWBS-aided systems, when fourth or eighth order CIR prediction filters are employed.

TABLE 4. MAP MUD and CE complexity (CFEs/bit) of the scenarios in Fig. 19 at BER = 10^{-5}.

N_{tap}	RWBS CE	QRWBS CE
0	-	103.40
1	-	103.87
2	103.30	101.85
4	108.80	102.71
8	108.62	103.95

The improved performance of the QRWBS-aided systems over the RWBS-aided systems is achieved at a lower complexity, as seen in Table 4. In Table 4 the joint complexity of the MAP MUD and the selected CE is presented for each scenario of Fig. 19, rather than showing only the complexity of the CE, since provided that the frame is correctly decoded during the first MUD-CE-DEC iteration, the Cyclic Redundancy Check (CRC) assumed will realize it and no further MUD-CE-DEC iterations will be needed. Therefore, the performance of the CE employed may affect the overall complexity of the system.

Let us now select $N_{tap} = 4$ for the order of the CIR prediction filter and vary the I_{CE}^{MUD} and I_{DEC}^{MUD-CE} number of iterations in our scenarios. Referring to the discussions in Section VI, in Fig. 20 we allow multiple MUD-CE iterations during every MUD-CE-DEC iteration, where we may observe that the performance is very similar to the corresponding scenarios, where multiple MUD-CE iterations are only allowed during the first MUD-CE-DEC iteration, but the complexity is increased according to Table 5, since more MUD and CE operations are performed. The QRWBS-aided CE performs better than the RWBS-aided CE in all the demonstrated scenarios, with the associated gain varying from 1.1 dB up to 2.5 dB, depending on the specific scenario.

As it was expected, according to Fig. 20, when we allow more iterations between the MUD and the CE, or the MUD-CE and the decoders, the performance is improved. It is also worth comparing the scenarios which have

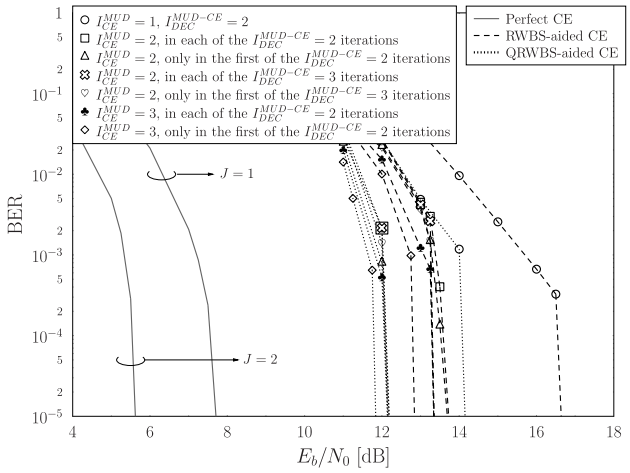

FIGURE 20. BER performance of an SDMA-OFDM system supporting $U = 4$ users with $P = 2$ receive AEs, transmitting over ETU channels, when perfect CE is available, as well as when the RWBS and the QRWBS are employed for CE. The CIR prediction filter's order is $N_{tap} = 4$ and various combinations of I_{CE}^{MUD} and I_{DEC}^{MUD-CE} iterations are allowed between the MAP MUD, the CE and the decoders. The interleaver length is 8 192 bits and a pilot OFDM symbol is transmitted every 8 data OFDM symbols. The rest of the parameters are stated in Table 2 and Table 3.

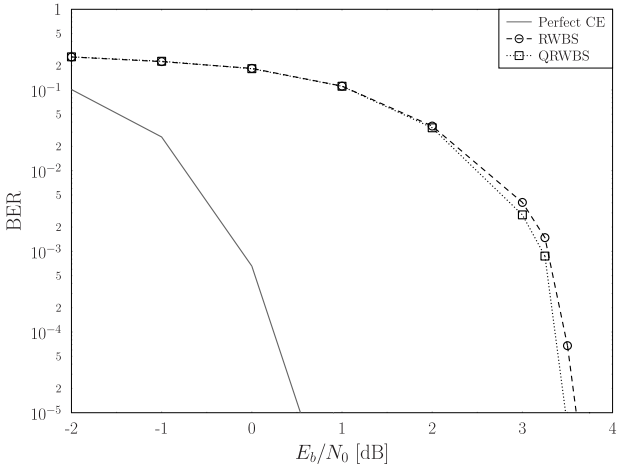

FIGURE 21. BER performance of an SDMA-OFDM system supporting $U = 4$ users with $P = 4$ receive AEs, transmitting over ETU channels, when perfect CE is available, as well as when the RWBS and the QRWBS are employed for CE. The CIR prediction filter's order is $N_{tap} = 4$, $I_{CE}^{MUD} = 1$ iteration is allowed between the MAP MUD and the CE and $I_{DEC}^{MUD-CE} = 1$ iteration is allowed between the MUD-CE and the decoders. The interleaver length is 8 192 bits and a pilot OFDM symbol is transmitted every 8 data OFDM symbols. The rest of the parameters are stated in Table 2 and Table 3.

TABLE 5. MAP MUD and CE complexity (CFEs/bit) of the scenarios in Fig. 20 at BER $= 10^{-5}$.

Multiple MUD-CE iterations during each MUD-CE-DEC iteration	I_{CE}^{MUD}	I_{DEC}^{MUD-CE}	RWBS CE	QRWBS CE
-	1	2	38.09	35.29
YES	2	2	82.07	77.84
NO	2	2	74.20	72.22
YES	2	3	83.88	79.49
NO	2	3	75.68	72.72
YES	3	2	117.52	111.42
NO	3	2	106.57	102.71

similar complexity. For example, the system associated with $I_{CE}^{MUD} = 3$ and $I_{DEC}^{MUD-CE} = 2$ employs the MAP MUD 4 times, the CE 3 times and the decoders twice, while the system using $I_{CE}^{MUD} = 2$ and $I_{CE}^{MUD} = 3$ employs the MAP MUD 4 times, the CE 3 times and the decoders 3 times. Therefore, the latter system employs the decoders one more time than the former system, but exhibits a performance loss of 0.2 dB, as illustrated in Fig. 20. This phenomenon is related to the essence of the DDCE, which is shown to perform better, when a better symbol estimate is available at the output of the MUD before we start the MUD-CE-DEC iterations. Hence, it may be worth investing more complexity in the MUD-CE iterations of the first MUD-CE-DEC iterations for increasing the chances of obtaining a multi-level symbol vector with fewer errors, which will allow the channel decoders to correct the remaining errors.

Next we demonstrate that the high power loss that the investigated RWBS-aided and QRWBS-aided CE scenarios exhibit with respect to the perfect CE scenarios is not a deficiency of the algorithms employed, but rather due to the systems being rank-deficient. Accordingly, in Fig. 21 we present the BER performance of the same system supporting $U = 4$ users transmitting over ETU channels, when $P = 4$ receive AEs are available at the BS, making it a full-rank system, when relying on a single activation of the MAP MUD. The same CE and the same decoders are used. The performance of the QRWBS-aided CE is slightly better than that of the RWBS-aided CE and the power loss with respect to the perfect CE scenario is approximately 3 dB. If multiple iterations were allowed between the MUD, the CE and the decoders, we should have expected the power loss to have been lower. The number of CFEs required by the QRWBS-aided CE was 8.89 CFEs per bit, while that of the RWBS-aided CE was 12 CFEs per bit, highlighting again the ability of the QRWBS-aided CE not only to perform better, but also to impose a lower complexity.

In Fig. 22 we investigate the effect that erroneous detected multi-level symbol vectors at the output of the MUD have on the performance of the system, as well as the effect that multiple iterations between the MUD and the CE during the first MUD-CE-DEC iteration have on the same performance. More specifically, Fig. 22 depicts the BER performance of a system, where $U = 4$ users are supported with the aid of $P = 2$ receive AEs at the BS, when transmitting over ETU channels associated with $F_d = 0.02$. A fourth-order CIR prediction filter has been employed and the performance of the hypothetical scenarios, when perfect CE is available or when error-free symbol vectors are available at the input of

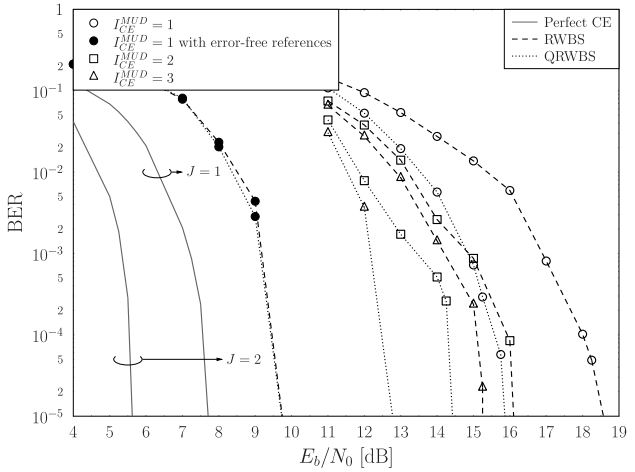

FIGURE 22. BER performance of an SDMA-OFDM system supporting $U = 4$ users with $P = 2$ receive AEs, transmitting over ETU channels, when perfect CE is available, as well as when the RWBS and the QRWBS are employed for CE with and without error-free symbol references. The CIR prediction filter's order is $N_{tap} = 4$ and various I_{CE}^{MUD} iterations are allowed between the MAP MUD and the CE, while only a single MUD-CE-DEC iteration is performed. The interleaver length is 8 192 bits and a pilot OFDM symbol is transmitted every 8 data OFDM symbols. The rest of the parameters are stated in Table 2 and Table 3.

the RWBS-aided and QRWBS-aided CE, are also presented. It should be noted that the error-free symbol references only affect the CE employed. Therefore, the MUD may output erroneous symbol vectors, based on the predicted CIR estimates, which are based on the previous OFDM symbols' CIR estimates.

In all the scenarios, the QRWBS-aided CE outperforms the RWBS-aided CE. Their complexity is similar, mainly because of the selection of $\Delta_\Xi = 10^{-4}$, which indicates that in these scenarios both the RWBS and the QRWBS converge at a similar speed, albeit the QRWBS-aided CE converges to a better CIR. Furthermore, at BER of 10^{-5}, the QRWBS-aided CE performs better in a scenario, where $I_{CE}^{MUD} = 1$ iterations are allowed between the MAP MUD and the CE, than the RWBS-aided CE in a scenario, where $I_{CE}^{MUD} = 2$ MUD-CE iterations are performed. Similarly, the QRWBS-aided CE operating in a scenario of $I_{CE}^{MUD} = 2$ outperforms the RWBS-aided CE relying on $I_{CE}^{MUD} = 3$. This affects the complexity of the scenarios, since an extra CE operation plus the extra MUD operation will highly increase the system's complexity, as exemplified in Table 6. Finally, the QRWBS-aided CE outperforms the RWBS-aided CE in the same scenarios by approximately 2.5 dB.

In the specific scenario, where no iterations are performed between the MAP MUD, the CE and the decoders, the QRWBS-aided CE requires 2.5 dB less power than the RWBS-aided scheme for achieving a BER of 10^{-5}. However, in the hypothetical scenario, where error-free symbol references were available at the input of the CE, a gain of 6 dB would be acquired at a BER of 10^{-5}, when compared to the QRWBS-aided CE scenario at the absence of error-free references.

TABLE 6. MAP MUD and CE complexity (CFEs/bit) of the scenarios in Fig. 22 at BER = 10^{-5}.

Error-Free Symbol References	I_{CE}^{MUD}	RWBS CE	QRWBS CE
NO	1	34.13	33.90
YES	1	35.27	34.90
NO	2	66.62	66.43
NO	3	98.90	98.05

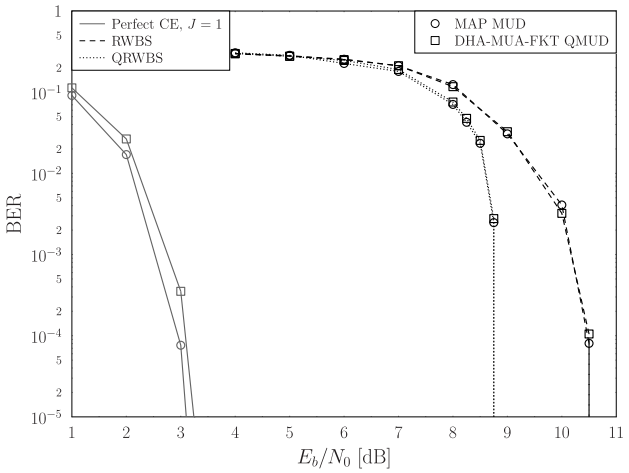

FIGURE 23. BER performance of an SDMA-OFDM system supporting $U = 7$ users with $P = 4$ receive AEs, transmitting over ETU channels, when perfect CE is available, as well as when the RWBS and the QRWBS are employed for CE. The CIR prediction filter's order is $N_{tap} = 4$ and $I_{CE}^{MUD} = 3$ iterations are allowed between the MAP MUD and the CE, while $I_{DEC}^{MUD-CE} = 2$ MUD-CE-DEC iterations are performed. The interleaver length is 8 192 bits and a pilot OFDM symbol is transmitted every 8 data OFDM symbols. The rest of the parameters are stated in Table 2 and Table 3.

Let us now investigate the BER performance of a rank-deficient system in Fig. 23, where $U = 7$ users are supported using $P = 4$ receive AEs available at the BS, when transmitting over ETU channels associated with $F_d = 0.02$. The MAP MUD and the DHA-MUA-FKT QMUD [30], [32] are employed, along with the RWBS-aided and the QRWBS-aided CE. We may observe that the DHA-MUA-FKT QMUD associated with perfect CE, as well as with RWBS-aided CE and QRWBS-aided CE performs near-optimally with respect to the MAP MUD, while requiring a lower number of CFEs according to Table 6. The QRWBS-aided CE provides a gain of approximately 2 dB with respect to the RWBS-aided CE, regardless of the choice of MUD, while it is 5 dB away of the scenario, where perfect CE is available. By comparing the difference in the computational complexities seen in Table 7 between the scenarios, where the RWBS-aided and QRWBS-aided CEs are used, to those of Table 4, Table 5 and Table 6, we may observe that the complexity gain between the classical CE and the quantum-assisted CE becomes higher when more users are supported by the system. It is worth mentioning that a purely quantum-assisted system, associated

TABLE 7. MAP MUD and CE complexity (CFEs/bit) of the scenarios in Fig. 23 at BER = 10^{-5}.

MUD / QMUD	Perfect CE	RWBS CE	QRWBS CE
MAP	1170.29	3587.76	3517.45
DHA-MUA-FKT	599.64	2127.74	2056.26

TABLE 8. BER performance and complexity summary of Fig. 23 at BER = 10^{-5}.

MUD / QMUD	CE / QCE	Distance from Perfect CE and MAP MUD at BER = 10^{-5} (dB)	Complexity at BER = 10^{-5} (CFEs)
DHA-MUA-FKT	Perfect CE	0.14	599.64
MAP	Perfect CE	0	1170.29
DHA-MUA-FKT	QRWBS	5.65	2056.26
DHA-MUA-FKT	RWBS	7.4	2127.74
MAP	QRWBS	5.65	3517.45
MAP	RWBS	7.4	3587.76

with the DHA-MUA-FKT QMUD and the QRWBS-aided CE not only achieves a 2 dB gain at a BER of 10^{-5} with respect to a purely classical system associated with the MAP MUD and the RWBS-aided CE, but also requires only 57.3% of its complexity, as observed in Table 7.

VIII. CONCLUSIONS

The QRWBS-aided DDCE was proposed and employed in the uplink of SDMA-OFDM systems. Its MSE and BER performance was compared to that of the RWBS-aided DDCE [17], [19] in conjunction with the MAP MUD and the DHA-MUA-FKT QMUD [30], [32]. In Fig. 9 we demonstrated that the proposed weighted boosting search performs better than the conventional weighted boosting search [17], while in Fig. 10 we compared the MSE performance of the proposed joint CE and MUD in EVA and ETU channels. The effect that the Doppler frequency has on the system's MSE performance in noiseless scenarios was characterized in Fig. 11, while Fig. 12 illustrates the MSE of the CE. Additionally, the effects of error propagation were demonstrated in Fig. 13, while the proposed QRWBS-aided DDCE was found to be superior, regardless of the number of received AEs in Fig. 14. In Fig. 15, we investigated the employment of the QRWBS in conjunction with various initial number of individuals. When increasing the number of users supported by the system, Fig. 16 and Fig. 17 showed that the QRWBS-aided CE still outperforms the RWBS-aided CE.

Based on Fig. 18, we may conclude that the QRWBS-aided and RWBS-aided CE is capable of exhibiting a performance closer to that of an idealized system, where perfect CE is available, provided that the Doppler frequency is low and the channels' PDP includes a low number of paths. Fig. 19 demonstrates that employing a CIR prediction filter improves the system's overall performance, regardless of the choice of the CE used and that the QRWBS-aided CE performs well even with a low-order CIR prediction filter or even in the absence of a CIR prediction filter, whilst the RWBS-aided CE experiences an error-floor due to error propagation. Furthermore, the effect that various combinations of iterations between the MUD and the CE, as well as the MUD, the CE and the DEC has on the system's BER performance was illustrated in Fig. 20. Based on Fig. 20, it may be beneficial to allow more MUD-CE iterations before employing the channel decoders for the first time.

Fig. 21 helps us conclude that the presented CE processes perform closer to the idealized systems, where perfect CE is available, when the number of receive AEs is equal to the number of users supported. By allowing only a single MUD-CE-DEC iteration, but multiple MUD-CE iterations, the QRWBS-aided CE still performs closer to the idealized system, where perfect CE is available, than the RWBS-aided CE, as evidenced by Fig. 22. In the same figure, the performance of the RWBS-aided and QRWBS-aided CEs are also quantified, when error-free symbol references are available at the input of the CE.

Finally, in Fig. 23 we characterized a rank-deficient system, where $U = 7$ users are supported and the DHA-MUA-FKT QMUD was employed. By using the QRWBS-aided CE a 2 dB gain is achieved with respect to the RWBS-aided CE, while the DHA-MUA-FKT QMUD achieves near-optimal performance, with respect to the MAP MUD, despite imposing a lower complexity. According to Table 4, Table 5, Table 6 and Table 7, the QRWBS-aided DDCE imposes a lower complexity than the RWBS-aided DDCE at a BER of 10^{-5}. Table 8 summarizes the complexity of Table 7 in conjunction with the BER performance of the rank-deficient multi-user system, associated with ETU channels and depicted in Fig. 23. It may be observed that the employment of the quantum-assisted MUD is the main contributor in lowering the overall complexity without degrading the performance, while the use of the quantum-assisted CE results in a performance gain with an additional small complexity reduction.

REFERENCES

[1] L. L. Hanzo, M. Münster, B. Choi, and T. Keller, *OFDM and MC-CDMA for Broadband Multi-User Communications, WLANs and Broadcasting*. New York, NY, USA: Wiley, 2003.
[2] L. L. Hanzo, Y. Akhtman, M. Jiang, and L. Wang, *MIMO-OFDM for LTE, WiFi and WiMAX: Coherent Versus Non-Coherent and Cooperative Turbo-Transceivers*. New York, NY, USA: Wiley, 2010.
[3] Y. Li, N. Seshadri, and S. Ariyavisitakul, "Channel estimation for OFDM systems with transmitter diversity in mobile wireless channels," *IEEE J. Sel. Areas Commun.*, vol. 17, no. 3, pp. 461–471, Mar. 1999.
[4] Y. Li, "Simplified channel estimation for OFDM systems with multiple transmit antennas," *IEEE Trans. Wireless Commun.*, vol. 1, no. 1, pp. 67–75, Jan. 2002.
[5] L. Hanzo, O. Alamri, M. El-Hajjar, and N. Wu, *Near-Capacity Multi-Functional MIMO Systems: Sphere-Packing, Iterative Detection and Cooperation*. New York, NY, USA: Wiley, May 2009.
[6] Y. G. Li, J. H. Winters, and N. R. Sollenberger, "MIMO-OFDM for wireless communications: Signal detection with enhanced channel estimation," *IEEE Trans. Commun.*, vol. 50, no. 9, pp. 1471–1477, Sep. 2002.

[7] P. Botsinis, S. X. Ng, and L. Hanzo, "Quantum search algorithms, quantum wireless, and a low-complexity maximum likelihood iterative quantum multi-user detector design," *IEEE Access*, vol. 1, pp. 94–122, 2013.
[8] M. Ghosh and C. L. Weber, "Maximum-likelihood blind equalization," *Opt. Eng.*, vol. 31, no. 6, pp. 1224–1228, 1992.
[9] N. Seshadri, "Joint data and channel estimation using blind trellis search techniques," *IEEE Trans. Commun.*, vol. 42, no. 234, pp. 1000–1011, Feb./Apr. 1994.
[10] S. Chen and Y. Wu, "Maximum likelihood joint channel and data estimation using genetic algorithms," *IEEE Trans. Signal Process.*, vol. 46, no. 5, pp. 1469–1473, May 1998.
[11] P. Zhang, S. Chen, and L. Hanzo, "Embedded iterative semi-blind channel estimation for three-stage-concatenated MIMO-aided QAM turbo transceivers," *IEEE Trans. Veh. Technol.*, vol. 63, no. 1, pp. 439–446, Jan. 2014.
[12] D. K. C. So and R. S. Cheng, "Iterative EM receiver for space-time coded systems in MIMO frequency-selective fading channels with channel gain and order estimation," *IEEE Trans. Wireless Commun.*, vol. 3, no. 6, pp. 1928–1935, Nov. 2004.
[13] A. Assra, W. Hamouda, and A. Youssef, "EM-based joint channel estimation and data detection for MIMO-CDMA systems," *IEEE Trans. Veh. Technol.*, vol. 59, no. 3, pp. 1205–1216, Mar. 2010.
[14] C. Novak, G. Matz, and F. Hlawatsch, "IDMA for the multiuser MIMO-OFDM uplink: A factor graph framework for joint data detection and channel estimation," *IEEE Trans. Signal Process.*, vol. 61, no. 16, pp. 4051–4066, Aug. 2013.
[15] R. Prasad, C. R. Murthy, and B. D. Rao, "Joint channel estimation and data detection in MIMO-OFDM systems: A sparse Bayesian learning approach," *IEEE Trans. Signal Process.*, vol. 63, no. 20, pp. 5369–5382, Oct. 2015.
[16] Y. Wu, X. Zhu, and A. K. Nandi, "Soft-input turbo channel estimation for single-carrier multiple-input–multiple-output systems," *IEEE Trans. Veh. Technol.*, vol. 58, no. 7, pp. 3867–3873, Sep. 2009.
[17] J. Zhang, S. Chen, X. Mu, and L. Hanzo, "Joint channel estimation and multiuser detection for SDMA/OFDM based on dual repeated weighted boosting search," *IEEE Trans. Veh. Technol.*, vol. 60, no. 7, pp. 3265–3275, Sep. 2011.
[18] M. Jiang, J. Akhtman, and L. Hanzo, "Iterative joint channel estimation and multi-user detection for multiple-antenna aided OFDM systems," *IEEE Trans. Wireless Commun.*, vol. 6, no. 8, pp. 2904–2914, Aug. 2007.
[19] J. Zhang, S. Chen, X. Mu, and L. Hanzo, "Evolutionary-algorithm-assisted joint channel estimation and turbo multiuser detection/decoding for OFDM/SDMA," *IEEE Trans. Veh. Technol.*, vol. 63, no. 3, pp. 1204–1222, Mar. 2014.
[20] J. Zhang, S. Chen, X. Mu, and L. Hanzo, "Turbo multi-user detection for OFDM/SDMA systems relying on differential evolution aided iterative channel estimation," *IEEE Trans. Commun.*, vol. 60, no. 6, pp. 1621–1633, Jun. 2012.
[21] M. A. Nielsen and I. L. Chuang, *Quantum Computation and Quantum Information*. Cambridge, U.K.: Cambridge Univ. Press, 2000.
[22] S. Imre and F. Balázs, *Quantum Computing and Communications: An Engineering Approach*. New York, NY, USA: Wiley, 2005.
[23] S. Imre and L. Gyongyosi, *Advanced Quantum Communications: An Engineering Approach*. New York, NY, USA: Wiley, 2013.
[24] L. K. Grover, "A fast quantum mechanical algorithm for database search," in *Proc. 28th Annu. ACM Symp. Theory Comput.*, May 1996, pp. 212–219.
[25] L. K. Grover, "Quantum mechanics helps in searching for a needle in a haystack," *Phys. Rev. Lett.*, vol. 79, pp. 325–328, Jul. 1997.
[26] M. Boyer, G. Brassard, P. Høyer, and A. Tapp, "Tight bounds on quantum searching," *Fortschritte Phys.*, vol. 46, nos. 4–5, pp. 493–506, 1998.
[27] C. Durr and P. Høyer. (Jul. 1996). "A quantum algorithm for finding the minimum." [Online]. Available: http://arxiv.org/abs/quant-ph/9607014
[28] A. Malossini, E. Blanzieri, and T. Calarco, "Quantum genetic optimization," *IEEE Trans. Evol. Comput.*, vol. 12, no. 2, pp. 231–241, Apr. 2008.
[29] P. Botsinis, S. X. Ng, and L. Hanzo, "Fixed-complexity quantum-assisted multi-user detection for CDMA and SDMA," *IEEE Trans. Commun.*, vol. 62, no. 3, pp. 990–1000, Mar. 2014.
[30] P. Botsinis, D. Alanis, S. X. Ng, and L. Hanzo, "Low-complexity soft-output quantum-assisted multiuser detection for direct-sequence spreading and slow subcarrier-hopping aided SDMA-OFDM systems," *IEEE Access*, vol. 2, pp. 451–472, May 2014.
[31] P. Botsinis, S.-X. Ng, and L. Hanzo, "Low-complexity iterative quantum multi-user detection in SDMA systems," in *Proc. IEEE Int. Conf. Commun. (ICC)*, Jun. 2014, pp. 5592–5597.
[32] P. Botsinis, D. Alanis, Z. Babar, S. X. Ng, and L. Hanzo, "Iterative quantum-assisted multi-user detection for multi-carrier interleave division multiple access systems," *IEEE Trans. Commun.*, vol. 63, no. 10, pp. 3713–3727, Oct. 2015.
[33] P. Botsinis, D. Alanis, Z. Babar, S. X. Ng, and L. Hanzo, "Noncoherent quantum multiple symbol differential detection for wireless systems," *IEEE Access*, vol. 3, no. 99, pp. 569–598, May 2015.
[34] D. Alanis, P. Botsinis, S. X. Ng, and L. Hanzo, "Quantum-assisted routing optimization for self-organizing networks," *IEEE Access*, vol. 2, pp. 614–632, Jun. 2014.
[35] D. Alanis, P. Botsinis, Z. Babar, S. X. Ng, and L. Hanzo, "Non-dominated quantum iterative routing optimization for wireless multihop networks," *IEEE Access*, vol. 3, pp. 1704–1728, 2015.
[36] S. Imre, "Quantum communications: Explained for communication engineers," *IEEE Commun. Mag.*, vol. 51, no. 8, pp. 28–35, Aug. 2013.
[37] Z. Babar, S. X. Ng, and L. Hanzo, "EXIT-chart-aided near-capacity quantum turbo code design," *IEEE Trans. Veh. Technol.*, vol. 64, no. 3, pp. 866–875, Mar. 2014.
[38] Z. Babar, P. Botsinis, D. Alanis, S. X. Ng, and L. Hanzo, "The road from classical to quantum codes: A hashing bound approaching design procedure," *IEEE Access*, vol. 3, pp. 146–176, 2015.
[39] Z. Babar, P. Botsinis, D. Alanis, S. X. Ng, and L. Hanzo, "Fifteen years of quantum LDPC coding and improved decoding strategies," *IEEE Access*, vol. 3, pp. 2492–2519, 2015.
[40] S. Chen, X. Wang, and C. J. Harris, "Experiments with repeating weighted boosting search for optimization signal processing applications," *IEEE Trans. Syst., Man, Cybern. B, Cybern.*, vol. 35, no. 4, pp. 682–693, Aug. 2005.
[41] S. Sesia, I. Toufik, and M. Baker, *LTE—The UMTS Long Term Evolution: From Theory to Practice*. New York, NY, USA: Wiley, 2009.

PANAGIOTIS BOTSINIS (S'12–M'15) received the M.Eng. degree from the School of Electrical and Computer Engineering, National Technical University of Athens, Greece, in 2010, the M.Sc. degree (Hons.), and the Ph.D. degree in wireless communications from the University of Southampton, U.K., in 2011 and 2015, respectively. He is currently a Research Fellow with the Southampton Wireless Group, School of Electronics and Computer Science, University of Southampton, U.K. Since 2010, he has been a member of the Technical Chamber of Greece. His research interests include quantum-assisted communications, quantum computation, iterative detection, OFDM, MIMO, multiple access systems, coded modulation, channel coding, cooperative communications, and combinatorial optimization.

DIMITRIOS ALANIS (S'13) received the M.Eng. degree in electrical and computer engineering from the Aristotle University of Thessaloniki in 2011, and the M.Sc. degree in wireless communications from the University of Southampton in 2012. He is currently pursuing the Ph.D. degree with the Southampton Wireless Group, School of Electronics and Computer Science, University of Southampton. His research interests include quantum computation and quantum information theory, quantum search algorithms, cooperative communications, resource allocation for selforganizing networks, bio-inspired optimization algorithms, and classical and quantum game theory.

ZUNAIRA BABAR received the B.Eng. degree in electrical engineering from the National University of Science and Technology, Islamabad, Pakistan, in 2008, and the M.Sc. degree (Hons.) and the Ph.D. degree in wireless communications from the University of Southampton, U.K., in 2011 and 2015, respectively. She is currently a Research Fellow with the Southampton Wireless Group, University of Southampton. Her research interests include quantum error correction codes, channel coding, coded modulation, iterative detection, and cooperative communications.

SOON XIN NG (S'99–M'03–SM'08) received the B.Eng. degree (Hons.) in electronics engineering and the Ph.D. degree in wireless communications from the University of Southampton, Southampton, U.K., in 1999 and 2002, respectively. From 2003 to 2006, he was a Post-Doctoral Research Fellow, where he is involved in collaborative European research projects known as SCOUT, NEWCOM, and PHOENIX. Since 2006, he has been a member of Academic Staff with the School of Electronics and Computer Science, University of Southampton. He is involved in the OPTIMIX and CONCERTO European projects and the IUATC and UC4G projects. He is currently an Associate Professor of Telecommunications with the University of Southampton. He has authored over 180 papers and co-authored two John Wiley/IEEE Press books in his research field. His research interests include adaptive coded modulation, coded modulation, channel coding, space-time coding, joint source and channel coding, iterative detection, OFDM, MIMO, cooperative communications, distributed coding, quantum error correction codes, and joint wireless-and-optical-fiber communications. He is a Chartered Engineer and a Fellow of the Higher Education Academy in the U.K.

LAJOS HANZO (M'91–SM'92–F'04) received the degree in electronics in 1976, and the doctorate in 1983. In 2009, he received the honorary doctorate Doctor Honoris Causa by the Technical University of Budapest. During his 38-year career in telecommunications, he has held various research and academic posts in Hungary, Germany, and the U.K. Since 1986, he has been with the School of Electronics and Computer Science, University of Southampton, U.K., where he holds the Chair in telecommunications. He has successfully supervised about 100 Ph.D. students. He has co-authored 20 John Wiley/IEEE Press books on mobile radio communications totalling in excess of 10,000 pages. He has published over 1,500 research entries at IEEE Xplore, as a TPC and the General Chair of the IEEE conferences, presented keynote lectures and has been awarded a number of distinctions. He is currently directing a 100-strong academic research team, where he is involved in a range of research projects in the field of wireless multimedia communications sponsored by industry, the Engineering and Physical Sciences Research Council U.K., the European Research Council's Advanced Fellow Grant, and the Royal Society's Wolfson Research Merit Award. He is an enthusiastic supporter of industrial and academic liaison and he offers a range of industrial courses. He is a fellow of the Royal Academy of Engineering, the Institution of Engineering and Technology, and the European Association for Signal Processing. He is also a Governor of the IEEE VTS. From 2008 to 2012, he was the Editor-in-Chief of the IEEE Press. He was a Chaired Professor with Tsinghua University, Beijing. He has over 22,000 citations.